Molecular Therapy
Methods & Clinical Development
Original Article

A Five-Repeat Micro-Dystrophin Gene Ameliorated Dystrophic Phenotype in the Severe DBA/2J-mdx Model of Duchenne Muscular Dystrophy

Chady H. Hakim,[1,2] Nalinda B. Wasala,[1] Xiufang Pan,[1] Kasun Kodippili,[1] Yongping Yue,[1] Keqing Zhang,[1] Gang Yao,[3] Brittney Haffner,[1] Sean X. Duan,[1] Julian Ramos,[4] Joel S. Schneider,[5] N. Nora Yang,[2] Jeffrey S. Chamberlain,[4] and Dongsheng Duan[1,3,6,7]

[1]Department of Molecular Microbiology and Immunology, School of Medicine, University of Missouri, Columbia, MO 65212, USA; [2]National Center for Advancing Translational Sciences (NCATS), Bethesda, MD 20892, USA; [3]Department of Bioengineering, University of Missouri, Columbia, MO 65212, USA; [4]Department of Neurology, Wellstone Muscular Dystrophy Research Center, University of Washington, Seattle, WA 98105, USA; [5]Solid Biosciences, LLC, Cambridge, MA 02142, USA; [6]Department of Neurology, School of Medicine, University of Missouri, Columbia, MO 65212, USA; [7]Department of Biomedical Sciences, College of Veterinary Medicine, University of Missouri, Columbia, MO 65212, USA

Micro-dystrophins are highly promising candidates for treating Duchenne muscular dystrophy, a lethal muscle disease caused by dystrophin deficiency. Here, we report robust disease rescue in the severe DBA/2J-mdx model with a neuronal nitric oxide synthase (nNOS)-binding micro-dystrophin vector. 2 × 10^{13} vector genome particles/mouse of the vector were delivered intravenously to 10-week-old mice and were evaluated at 6 months of age. Saturated micro-dystrophin expression was detected in all skeletal muscles and the heart and restored the dystrophin-associated glycoprotein complex and nNOS. In skeletal muscle, therapy substantially reduced fibrosis and calcification and significantly attenuated inflammation. Centronucleation was significantly decreased in the tibialis anterior (TA) and extensor digitorum longus (EDL) muscles but not in the quadriceps. Muscle function was normalized in the TA and significantly improved in the EDL muscle. Heart histology and function were also evaluated. Consistent with the literature, DBA/2J-mdx mice showed myocardial calcification and fibrosis and cardiac hemodynamics was compromised. Surprisingly, similar myocardial pathology and hemodynamic defects were detected in control DBA/2J mice. As a result, interpretation of the cardiac data proved difficult due to the confounding phenotype in control DBA/2J mice. Our results support further development of this microgene vector for clinical translation. Further, DBA/2J-mdx mice are not good models for Duchenne cardiomyopathy.

INTRODUCTION

Dystrophin is a large subsarcolemmal protein essential for muscle health. Out-of-frame mutations in the dystrophin gene abort dystrophin expression. The absence of dystrophin leads to Duchenne muscular dystrophy (DMD), an X-linked lethal debilitating muscle disease. Restoration of dystrophin expression in muscle cells by gene therapy will address the fundamental problem of dystrophin deficiency in DMD. A number of highly promising strategies are currently under development to replace or repair the mutated dystrophin gene or message RNA.[1–3] Adeno-associated virus (AAV)-mediated micro-dystrophin gene therapy stands out as an extremely attractive approach due to the AAV vector's unique capability for bodywide muscle transduction.[4] Encouragingly, AAV gene therapy has resulted in unequivocal clinical successes in treating other inherited diseases such as Leber congenital amaurosis, hemophilia, and spinal muscular atrophy.[5,6]

AAV is a single-stranded DNA virus with a packaging capacity of ~5 kb.[7] This creates a challenge for dystrophin gene delivery because the dystrophin coding sequence exceeds 11 kb. Full-length dystrophin contains four major structural domains, including the amino-terminal, rod, cysteine-rich, and C-terminal domains. The rod domain can be further divided into 24 spectrin-like repeats and four hinges. Some portions of these domains encode motifs for dystrophin to interact with the sarcolemma, extracellular matrix (via dystroglycan), cytoskeleton (actin microfilament, intermediate filament, and microtubule), and neuronal nitric oxide synthase (nNOS).

In the early 1990s, England et al.[8] found that some naturally occurring rod domain-truncated dystrophins are highly functional, suggesting that not all internal segments of dystrophin are essential. A subsequent study by Crawford et al.[9] showed that removal of the C-terminal domain has minimal impact on mouse muscle function. Based on these findings, investigators have generated rod domain-abbreviated and C-terminal domain-deleted micro-dystrophins that are about one-third the size of the full-length protein.[10,11] Importantly,

Received 3 April 2017; accepted 24 June 2017;
http://dx.doi.org/10.1016/j.omtm.2017.06.006.

Correspondence: Dongsheng Duan, PhD, Department of Molecular Microbiology and Immunology, School of Medicine, University of Missouri, One Hospital Dr., Columbia, MO 65212, USA.
E-mail: duand@missouri.edu

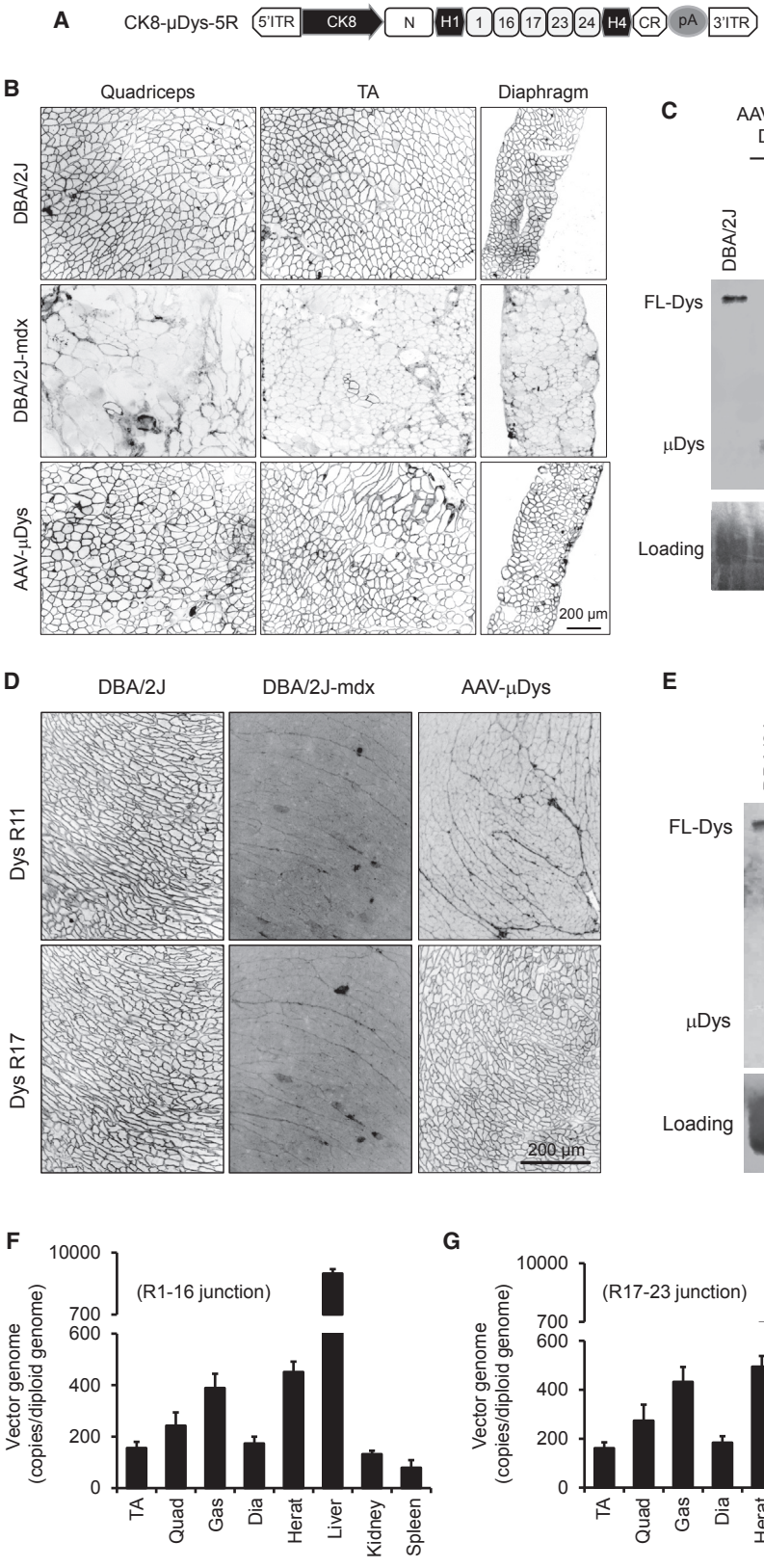

(legend on next page)

microgenes are less than 4 kb and can fit into an AAV particle. Local or systemic delivery of these micro-dystrophin AAV vectors greatly ameliorates muscle disease in mouse models of DMD.[10–14]

Despite these encouraging reports, the early versions of micro-dystrophin could not anchor nNOS to the sarcolemma.[15] The loss of sarcolemmal nNOS has been recognized as a critical pathogenic factor in DMD.[16,17] A microgene capable of normalizing nNOS localization would be highly preferable for DMD gene therapy. We recently discovered that dystrophin spectrin-like repeats 16 and 17 (R16/17) are the long-sought-after nNOS-binding domain.[18,19] We engineered several 6- to 8-kb R16/17-containing mini-dystrophin genes and demonstrated their therapeutic efficacy in mildly affected mdx and mdx4cv mice.[18,20,21] As an initial step toward the development of nNOS-binding micro-dystrophin gene therapy, we expressed a four-repeat R16/17-containing microgene from the ubiquitous cytomegalovirus (CMV) promoter in mdx mice via AAV-mediated gene transfer.[22] We obtained the expected sarcolemmal nNOS restoration, amelioration of pathology, and muscle function improvement.[22] While the results were encouraging, the vector was not ideal for human use (e.g., the use of the CMV promoter). To further establish the therapeutic utility of AAV-mediated nNOS-binding microgene therapy and in preparation for future clinical trials, we engineered a new vector. In this vector, a five-repeat R16/17-containing microgene was expressed from a muscle-specific CK8 promoter.[1,23] The construct was packaged in AAV serotype-9 (AAV-9) and delivered via the tail vein to 10-week-old DBA/2J-mdx mice, a recently developed severe mouse model for DMD.[24,25] At 15 weeks after AAV injection, we examined micro-dystrophin expression, dystrophin-associated/related proteins, histology, and skeletal muscle and heart function. Saturated skeletal muscle and heart transduction was observed in every treated animal. Micro-dystrophin greatly ameliorated skeletal muscle pathology and enhanced skeletal muscle function. Unexpectedly, we observed significant cardiomyopathy in control DBA/2J mice, limiting our ability to thoroughly evaluate heart rescue in treated animals.

RESULTS

Systemic AAV-9 Delivery Resulted in Robust Bodywide Micro-Dystrophin Expression in Muscles of DBA/2J-mdx Mice

The microgene construct used in this study has several unique features. Expression is driven by the muscle-specific CK8 promoter. The rod domain of micro-dystrophin contains five repeats (R1, R16, R17, R23, and R24) and two hinges (H1 and H4) (Figure 1A). The AAV-9 micro-dystrophin vector was delivered intravenously to five 10-week-old male and five 10-week-old female DBA/2J-mdx mice at the dose of 2×10^{13} vector genome (vg) particles/mouse. At 15 weeks after AAV injection, we examined micro-dystrophin expression and AAV genome distribution. On immunofluorescence staining, we observed saturated micro-dystrophin expression in all skeletal muscles in every treated mouse (Figure 1B; see also Figure S1A). The heart was also completely transduced (Figure 1D; see also Figure S1B). Western blot analysis confirmed high-level micro-dystrophin expression in both the skeletal muscle and the heart (Figures 1C and 1E). Quantification of the AAV genome copy number revealed accumulation of most of the vg in the liver, as expected from intravenous delivery. Nevertheless, approximately 150–500 copies/diploid genome of the vg were detected in the skeletal muscle and the heart (Figures 1F and 1G; see also Figure S1C).

Micro-Dystrophin Normalized nNOS Localization and Enhanced Recruitment of Other Components of the Dystrophin-Associated Glycoprotein Complex to the Sarcolemma

Dystrophin recruits a number of transmembrane (e.g., dystroglycans and sarcoglycans) and cytosolic (e.g., syntrophin and dystrobrevin) proteins into the dystrophin-associated glycoprotein complex (DGC). Dystrophin anchors nNOS to the sarcolemma in skeletal muscle.[18,19] We evaluated DGC restoration and nNOS expression by immunostaining on serial muscle sections (Figure 2). Epitope-specific dystrophin monoclonal antibodies confirmed the presence of R17 and absence of R11 in the skeletal muscle (Figure 2A) and heart (Figures 1D and 2C) of the AAV-injected DBA/2J-mdx mouse. In situ nNOS activity staining revealed successful sarcolemmal localization of enzymatically active nNOS in skeletal muscle following AAV micro-dystrophin therapy (Figure 2A). All components of the DGC were greatly diminished at the sarcolemma of untreated DBA/2J-mdx skeletal muscle (Figure 2B). Their expression was restored following AAV micro-dystrophin therapy (Figure 2B). DGC components in the heart of untreated DBA/2J-mdx mice were also reduced but appeared to be to a lesser extent compared to that of skeletal muscle (Figure 2C). After AAV micro-dystrophin therapy, the immunostaining intensity of the DGC was greatly enhanced in the heart (Figure 2C).

Figure 1. Systemic AAV-9 Injection Leads to Robust Expression of a Five-Repeat Micro-Dystrophin Gene in the Skeletal Muscle and Heart of DBA/2J-mdx Mice

(A) Schematic illustration of the AAV microgene vector. Micro-dystrophin consists of the N-terminal domain, two hinges (H1 and H4), five spectrin-like repeats (R1, R16, R17, R23, and R24), and the cysteine-rich (CR) domain. Micro-dystrophin expression is regulated by the muscle-specific CK8 promoter. (B) Representative dystrophin immunostaining photomicrographs demonstrating widespread microgene expression in the quadriceps, TA muscle, and diaphragm in treated DBA/2J-mdx mice. (C) A representative dystrophin western blot showing micro-dystrophin (μDys) at the expected size in AAV-treated muscles. (D) Representative immunostaining photomicrographs demonstrating robust myocardial micro-dystrophin expression in treated DBA/2J-mdx mice. Full-length dystrophin in the control DBA/2J heart reacted with both R11- and R17-specific antibodies. Therapeutic micro-dystrophin was recognized by the R17-specific but not the R11-specific antibody. (E) A representative dystrophin western blot showing abundant μDys at the expected size in the heart of treated DBA/2J-mdx mice. (F) Quantitative evaluation of AAV genome distribution in muscle and internal organs using in AAV microgene-injected female DBA/2J-mdx mice (n = 5). TaqMan qPCR detects the junction of R1-R16. Error bars are mean ± SEM. (G) Quantitative evaluation of AAV genome distribution in muscle and internal organs using in AAV microgene-injected female DBA/2J-mdx mice (n = 5). Error bars are mean ± SEM. TaqMan qPCR detects the junction of R17-R23. Dia, diaphragm; FL-Dys, full-length dystrophin; Gas, gastrocnemius; ITR, inverted terminal repeat; Quad, quadriceps; TA, tibialis anterior.

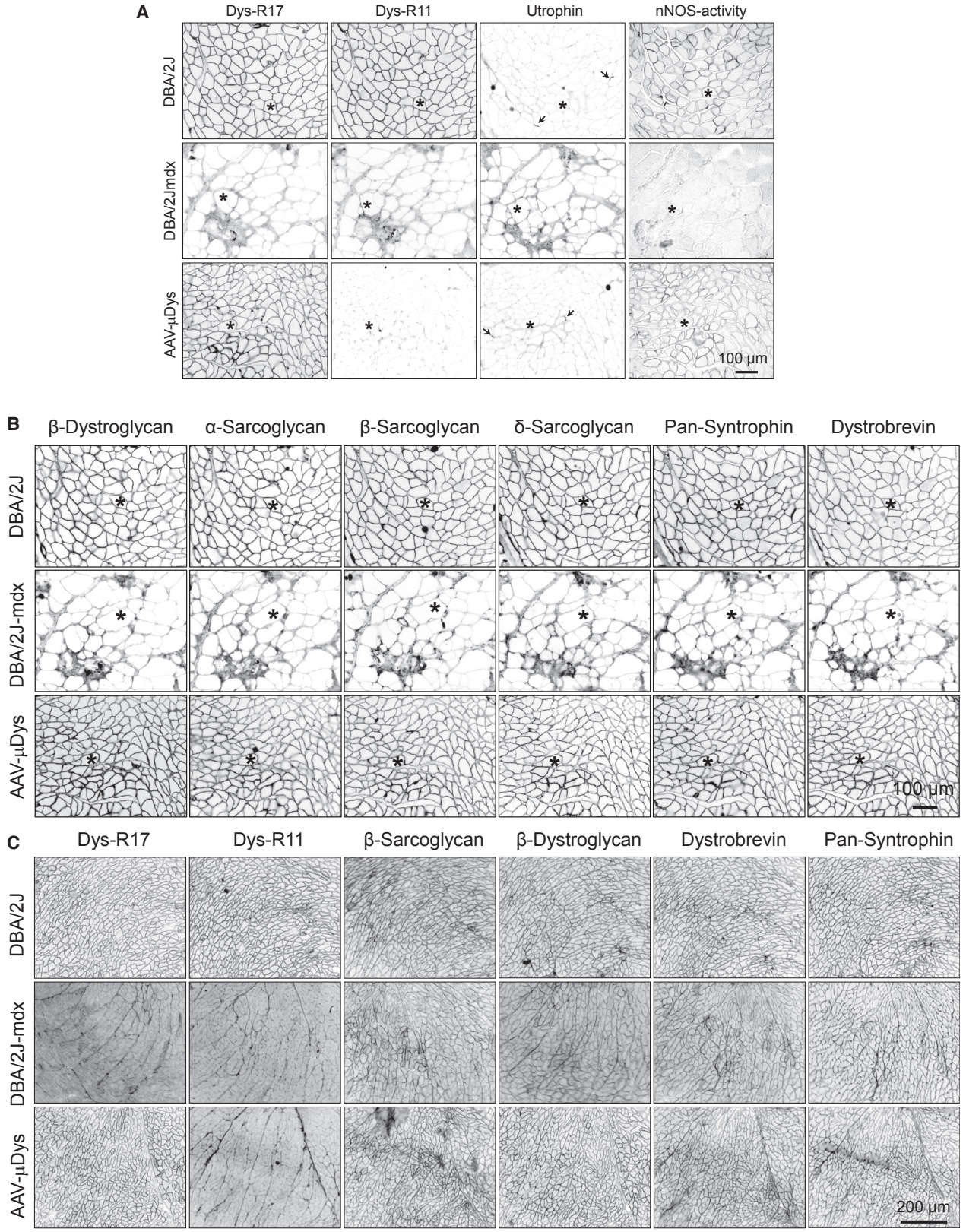

(legend on next page)

Utrophin is a dystrophin-related protein. In DBA mice, utrophin was mainly concentrated at the neuromuscular junctions (Figure 2A). Utrophin expression was moderately upregulated at the sarcolemma of untreated DBA/2J-mdx mice (Figure 2A). Micro-dystrophin appeared to have reduced sarcolemmal utrophin expression in DBA/2J-mdx mice (Figure 2A). Utrophin expression at the neuromuscular junction was not altered following micro-dystrophin therapy (Figure 2A).

Micro-Dystrophin Ameliorated Skeletal Muscle Pathology

On H&E staining, untreated DBA/2J-mdx mouse muscle showed characteristic dystrophic pathology, such as centrally localized nuclei, a large variety in myofiber size, and infiltration of mononuclear cells (Figures 3A; see also Figure S2). These pathologic lesions were clearly reduced following AAV micro-dystrophin therapy (Figure 3A; see also Figure S2). Masson trichrome staining and alizarin red staining revealed extensive interstitial fibrosis (blue color) and frequent appearance of calcified myofibers (dark red color), respectively, in untreated DBA/2J-mdx mouse muscle (Figure 3A). Fibrosis and calcification were all mitigated in AAV micro-dystrophin-treated muscle (Figure 3A).

To characterize inflammation, we performed immunohistochemistry staining using antibodies specific for macrophages and neutrophils. Patches of dark-brown stained macrophages and neutrophils were present throughout the muscle section in untreated DBA/2J-mdx mice but were barely visible in muscle of AAV micro-dystrophin-treated DBA/2J-mdx mice (Figure 3B). On quantification, macrophage and neutrophil numbers were significantly elevated in untreated DBA/2J-mdx muscle (Figure 3B). AAV treatment resulted in a significant reduction of these inflammatory cells.

To better appreciate the protective effect of micro-dystrophin, we performed morphometric quantification on the distribution of the myofiber size and the percentage of myofibers with centrally localized myonuclei in three representative limb muscles, including the quadriceps, tibialis anterior (TA), and extensor digitorum longus (EDL) muscle (Figures 3C and 3D). Compared to that of DBA/2J mice, the distribution of the myofiber size in untreated DBA/2J-mdx mice showed a marked leftward shift, indicating the presence of high numbers of small-size myofibers in dystrophic limb muscles (Figure 3C). The right end tail of the fiber size curve was elevated and spread farther in untreated DBA/2J-mdx mice, suggesting that they also have more large-size myofibers (Figure 3C). AAV micro-dystrophin therapy corrected the abnormal fiber size distribution to different extents in different muscles. It was nearly normalized in the EDL muscle but only partially improved in the quadriceps and TA muscle (Figure 3C). Central nucleation is a hallmark of muscle degeneration/regeneration. In untreated DBA/2J-mdx mice, ~40% of myofibers contained centrally localized nuclei (Figure 3D). AAV micro-dystrophin treatment significantly reduced centronucleation to approximately 30% in the TA and EDL muscle. Interestingly, there was no difference in the number of centrally nucleated myofibers in the quadriceps between treated and untreated DBA/2J-mdx mice (Figure 3D).

Micro-Dystrophin Normalized Skeletal Muscle Function

To thoroughly evaluate physiological consequences of micro-dystrophin therapy, we evaluated skeletal muscle force using two different approaches, including the ex vivo assay of the freshly dissected EDL muscle and the in situ assay of the TA muscle in live mice. On immunostaining, we observed saturated micro-dystrophin expression in both EDL and TA muscles (Figures 1B, S1, and S3). The EDL muscle of untreated DBA/2J-mdx mice showed significant atrophy, as demonstrated by the reduced muscle weight and cross-sectional area (CSA) (Table 1). Absolute twitch and tetanic forces of the untreated DBA/2J-mdx EDL muscle were significantly lower than those of the control DBA/2J EDL muscle (Figure S4). These deficiencies were almost completely corrected in AAV-treated mice (Figure S4). Specific twitch and tetanic forces of the EDL muscle in untreated DBA/2J-mdx mice were reduced by ~50% compared to those of control DBA/2J mice. Micro-dystrophin therapy fully normalized specific forces in the EDL muscle (Figure 4A). Force reduction following consecutive cycles of eccentric contraction is a highly sensitive index for studying dystrophic muscle function.[12,26,27] The control DBA/2J mouse EDL muscle was able to maintain ~80% of the force following 10 cycles of eccentric contraction stress (Figure 4A). Muscle force dropped dramatically during the first five cycles of eccentric contraction in the EDL muscle of untreated DBA/2J-mdx mice. Interestingly, force reduction became less apparent thereafter (Figure 4A). Micro-dystrophin-treated DBA/2J-mdx mice showed an eccentric contraction profile essentially identical to that of control DBA/2J mice (Figure 4A).

In situ examination of the TA muscle function yielded similar but slightly different results. The muscle weight and CSA of untreated DBA/2J-mdx mice were reduced compared to those of control DBA/2J mice but to a lesser extent compared to what was observed in the EDL muscle (Table 1). Absolute and specific forces of untreated DBA/2J-mdx mice were significantly lower than those of control DBA/2J mice (Figure 4B; see also Figure S4). Micro-dystrophin therapy normalized absolute and specific twitch forces in DBA/2J-mdx mice (Figure 4B; see also Figure S4). Absolute and specific tetanic forces were significantly improved but did not reach those

Figure 2. Five-Repeat Micro-Dystrophin Improves Sarcolemmal Localization of Dystrophin-Associated Glycoprotein Complex and Restores Membrane-Associated nNOS Activity

(A) Representative photomicrographs of dystrophin R17 and R11 immunostaining, utrophin immunostaining, and nNOS activity staining. Asterisks indicate the same myofiber in serial skeletal muscle sections. Arrows indicate the neuromuscular junction. (B) Representative photomicrographs of β-dystroglyan, α-sarcoglycan, β-sarcoglycan, δ-sarcoglycan, pan-syntrophin, and dystrobrevin from the same serial muscle sections shown in (A). (C) Representative photomicrographs of dystrophin R17 and R11, β-dystroglyan, β-sarcoglycan, pan-syntrophin, and dystrobrevin in the heart.

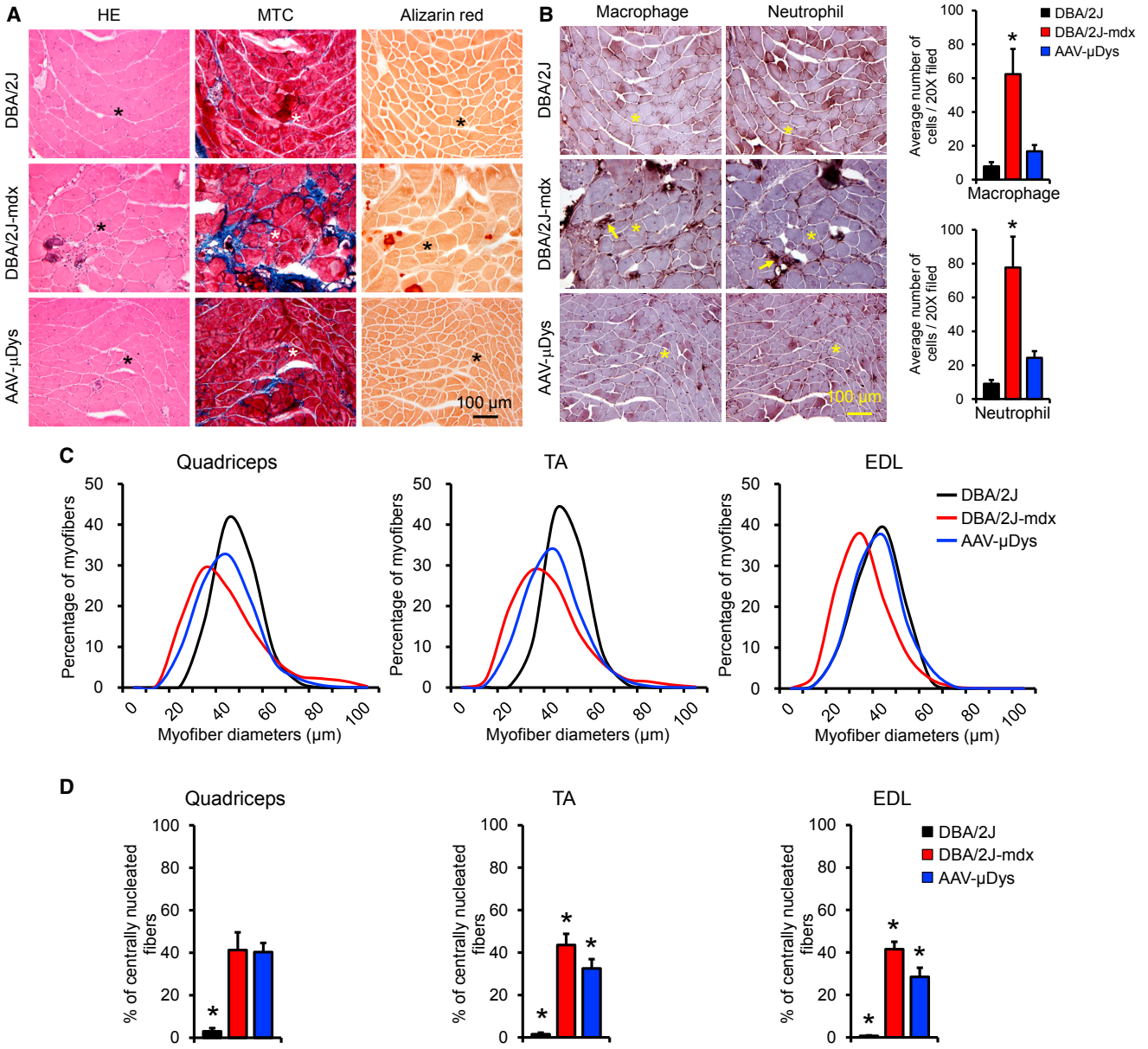

Figure 3. Five-Repeat Micro-Dystrophin Ameliorates Dystrophic Pathology in Skeletal Muscle of DBA/2J-mdx Mice

(A) Representative photomicrographs of H&E (HE), Masson trichrome (MTC), and alizarin red staining. The blue color in MTC staining indicates fibrosis. The dark red color in alizarin red staining marks calcification. (B) Representative photomicrographs of macrophage and neutrophil immunohistochemical staining from the same serial sections shown in (A). Arrows mark inflammatory cells. Bar graphs show macrophage and neutrophil quantification. Error bars are mean ± SEM. (C) Myofiber size distribution in the quadriceps, tibialis anterior muscle (TA), and extensor digitorum longus muscle (EDL). (D) Quantification of the proportion of centrally nucleated myofibers. Error bars are mean ± SEM. Asterisks in photomicrographs indicate the same myofiber in serial sections. Asterisks in bar graphs indicate significantly different from other groups.

of control DBA/2J mice (Figure 4B; see also Figure S4). In the eccentric contraction assay, we detected minimal force reduction in AAV micro-dystrophin-treated DBA/2J-mdx mice. In sharp contrast, there was a large force reduction in untreated DBA/2J-mdx mice (Figure 4B).

Absence of Dystrophin Did Not Cause Appreciable Alterations in the Heart Pathology of DBA/2J Mice

A recent study reported an absence of heart pathology in 7- to 52-week-old DBA/2J mice.[24] However, others have demonstrated myocardial calcification and inflammation as early as 4 weeks of

Table 1. Anatomic Properties of the Experimental Muscles

Muscle	Strain	n	Body Weight (g)	Muscle Weight (mg)	Lo (mm)	CSA (mm^2)
EDL						
	DBA/2J	10	28.22 ± 0.48[a]	10.36 ± 0.32[a]	13.08 ± 0.08[a]	1.71 ± 0.05[a]
	DBA/2J-mdx	8	24.50 ± 0.58	7.31 ± 0.25[b]	13.70 ± 0.15	1.15 ± 0.04[b]
	DBA/2J-mdx treated	5	25.00 ± 0.76	8.80 ± 0.24	13.98 ± 0.07	1.35 ± 0.03
TA						
	DBA/2J	5	27.28 ± 1.11	40.22 ± 1.16	14.67 ± 0.05	4.33 ± 0.12
	DBA/2J-mdx	8	24.41 ± 0.52	37.38 ± 1.43	14.78 ± 0.17[b]	3.99 ± 0.13
	DBA/2J-mdx treated	5	25.00 ± 0.76	38.12 ± 1.00	14.14 ± 0.07	4.25 ± 0.11

Data are presented as means ± SEM. CSA, cross-sectional area; EDL, extensor digitorum longus; Lo, optimal muscle length; TA, tibialis anterior.
[a]Significantly different from both untreated and AAV-treated DBA/2J-mdx mice.
[b]Significantly different from DBA/2J and AAV-treated DBA/2J-mdx.

age in DBA/2 mice.[28–30] We observed readily visible calcification and/or fibrosis on the surface of the DBA/2J but not C57Bl/10 mouse heart (Figure S5A). Consistent with previous publications,[28–30] epicardial calcified/fibrotic lesions in DBA/2J mice were primarily located on the surface of the right ventricle (Figure 5A; see also Figure S5A). Sporadic lesions of myocardial fibrosis and calcification were also observed in the septum and left ventricle (Figure 5; see also Figure S5B). Cardiac lesions were found not only in DBA/2J mice generated from in-house breeding but also in mice directly ordered from The Jackson Laboratory. Similar pathological changes were detected in the heart of untreated and AAV micro-dystrophin-treated DBA/2J-mdx mice (Figure 5; see also Figure S5B).

Impact of AAV Micro-Dystrophin Gene Therapy on Cardiac Function in DBA/2J-mdx Mice

We previously showed that dystrophin-deficient female mice can better model Duchenne cardiomyopathy seen in human patients.[31] Hence, we evaluated anatomic properties, electrophysiology, and cardiac hemodynamics in female mice. The body weight (BW), TA muscle weight (TW), heart weight (HW), and ventricle weight (VW) of untreated DBA/2J-mdx mice were significantly lower than those of control DBA/2J mice (Table 2). Micro-dystrophin-treated mice showed a significant increase in these weights (Table 2). DBA/2J-mdx mice had a significantly higher HW/BW ratio and VW/BW ratio than control DBA/2J mice. Micro-dystrophin therapy did not change these ratios (Table 2). The HW/TW and VW/TW ratios of DBA/2J-mdx mice were significantly higher than those of control DBA/2J mice. There was a trend of reduction in these two ratios in micro-dystrophin-treated DBA/2J-mdx mice, although it did not reach statistical significance (Table 2). The tibia length (TL) was not affected by muscle disease. Hence, the TL normalized heart weight ratio (HW/TL) and ventricle weight ratio (VW/TL) were considered better indicators of heart disease in the case of muscular dystrophy.[32] Interestingly, the HW/TL and VW/TL ratios were significantly reduced in DBA/2J-mdx mice. These ratios were significantly increased per the Mann-Whitney test in AAV-treated DBA/2J-mdx mice (Table 2).

Untreated DBA/2J-mdx mice displayed several electrocardiographic (ECG) features often seen in dystrophin-deficient mammals such as a significant reduction in the PR interval, significant prolongation of the QRS duration and QTc interval, and an increase in the cardiomyopathy index (Figures 6A and S6A).[33,34] Interestingly, DBA/2J-mdx mice did not show statistically significant tachycardia. Their heart rate was only slightly increased over that of DBA/2J mice (Figure 6A). Unexpectedly, the Q wave of DBA/2J mice was significantly deeper than that of DBA/2J-mdx mice (Figure 6A). AAV micro-dystrophin therapy did not lead to statistically significant improvement, although a trend of improvement was detected in several parameters, including the QRS duration, QTc interval, and cardiomyopathy index (Figure 6A).

On the cardiac catheter assay, there were no statistically significant differences in systolic parameters (end systolic volume, maximum pressure, and rate of rise of left ventricular pressure during heart contraction [dP/dt] max) and two diastolic parameters (end-diastolic volume and relaxation constant tau) among three experimental groups (Figure 6B; see also Figure S6B). The only statistically significant difference was dP/dt min. The absolute value of dP/dt min in DBA/2J mice was significantly larger than that of two other groups (Figure 6B; see also Figure S6B). Importantly, we did not see a statistically significant difference in indices for overall heart pump function (stroke volume, ejection fraction, and cardiac output) among three experimental groups (Figure 6B; see also Figure S6B).

DISCUSSION

To generate potentially supportive preclinical data for a new DMD clinical gene therapy program,[1,2] here we evaluated systemic AAV-9 micro-dystrophin therapy using a novel expression construct in severely affected DBA/2J-mdx mice. We observed highly efficient whole-body gene transfer and restoration of the DGC (including nNOS) by micro-dystrophin. In skeletal muscle, our treatment significantly reduced histological lesions and enhanced contractility. A recent study suggests that the DBA/2J-mdx mouse is a good model for DMD heart disease.[24] Surprisingly, we noticed clear cardiac

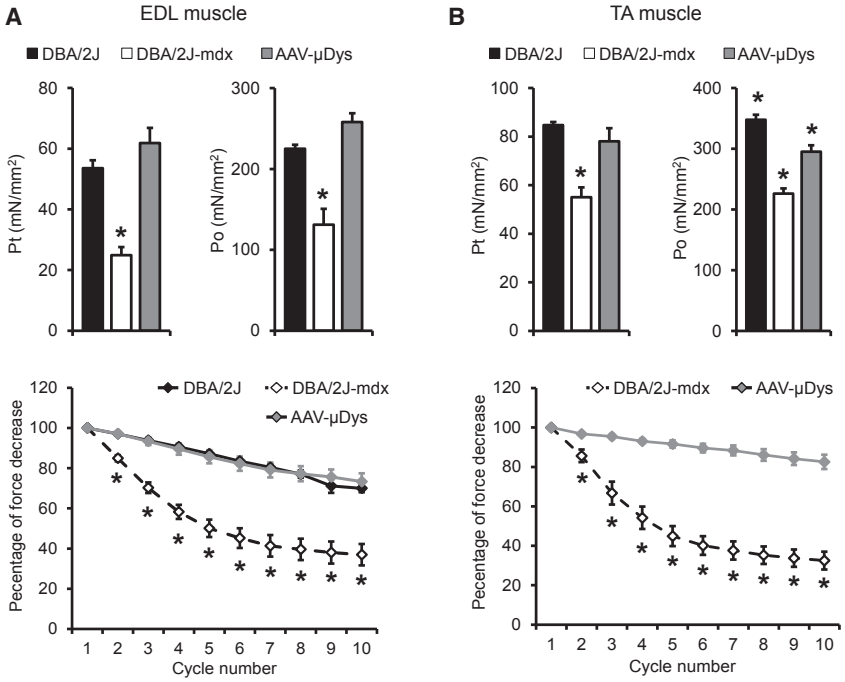

Figure 4. Five-Repeat Micro-Dystrophin Enhances Skeletal Muscle Function of DBA/2J-mdx Mice

(A) Quantitative evaluation of muscle contractility in the extensor digitorum longus (EDL) muscle. (Top Panel) Specific twitch (Pt) and tetanic (Po) forces. (Bottom Panel) Eccentric contraction profile. Error bars are mean ± SEM. (B) Quantitative evaluation of muscle contractility in the tibialis anterior (TA) muscle. (Top Panel) Specific twitch and tetanic forces. (Bottom Panel) Eccentric contraction profile. Error bars are mean ± SEM. Asterisks indicate significantly different from other group(s).

lesions in control DBA/2J mice and a lack of differences in heart pump function between DBA/2J and DBA/2J-mdx mice. Thus, despite supra-physiological expression of micro-dystrophin in the heart of treated DBA/2J-mdx mice, we were unable to reach a conclusion on cardiac rescue.

The large size of the dystrophin cDNA has been a major hurdle for AAV-mediated DMD gene replacement therapy. Despite the invention of dual and tri-vector systems for delivering the half-size and full-length dystrophin cDNA, these technologies are still in the early development stage and are not ready for clinical translation.[20,21,35–39] On the other side, a phase I trial has been conducted to deliver a highly shrunk micro-dystrophin gene by direct muscle injection.[40] To develop single AAV gene therapy for DMD, researchers have invented synthetic microgenes that carry only one-third of the dystrophin coding sequence.[10,11,18] These microgenes contain one to five spectrin-like repeats and many can effectively reduce muscle pathology and improve muscle function in dystrophic mice when delivered by AAV.[10–12,14,41] Importantly, our recent studies suggest that AAV microgene therapy protects muscle in large mammals afflicted by DMD.[22,42] In support of our results, Baroncelli et al.[43] found that naturally existing micro-dystrophin is associated with the mild Becker form of muscular dystrophy. Collectively, existing evidence justifies further development of AAV microgene therapy to treat human patients. With this backdrop, we initiated this study.

Several factors were considered in the design of this study. First, we designed a new expression cassette distinctive from the existing constructs. We used a novel muscle-specific CK8 promoter to drive strong expression in both skeletal muscle and cardiac muscle.[1,23] More than 30 different micro-dystrophin genes have been tested. The major difference in these microgenes is in the rod domain. In this regard, we opted to pursue a novel microgene that contains the R16/17 nNOS-binding domain. As homeostasis of nNOS is disrupted in DMD and in light of the critical role that nNOS plays in muscle regeneration, metabolism, mitochondria biogenesis, blood flow, and contraction,[44–47] it is critical to normalize nNOS homeostasis. Validation of the mouse data in affected dogs sets the foundation for treating dystrophic large mammals, including human patients. Species-related immune rejection has been a major confounding factor in gene therapy performed in the canine model.[48] In preparation for the subsequent dog study, and as an early readout for transgene efficacy, we have opted to use the canine microgene in our study. This canine construct had identical composition to a human construct (μDys5) currently in preclinical development (J.R. and J.C., unpublished data).

Second, we performed systemic delivery with AAV-9. In DMD, all body muscles are affected. An effective gene therapy for DMD will have to depend on efficient whole-body muscle transduction. A number of newly developed AAV serotypes are capable of bodywide systemic gene delivery following intravascular injection.[4] Among these, AAV-9 stands out as an extremely attractive candidate for systemic DMD gene therapy. AAV-9 was originally isolated from human tissues.[49] Subsequent studies have revealed efficient whole-body muscle transduction in rodents and dogs.[50–52] Furthermore, AAV-9-mediated systemic gene therapy significantly ameliorates disease phenotype in murine and canine models of DMD.[42,53,54] Importantly, an ongoing clinical trial on spinal muscular atrophy suggests that systemic AAV-9 gene therapy can be used to treat severely affected human patients without causing major adverse reactions.[6]

Third, we evaluated therapeutic efficacy in DBA/2J-mdx mice, a newly developed model that is thought to better phenocopy DMD than the commonly used mdx mice.[24,25] Although DMD mainly affects boys, dystrophin-deficient animals of both genders can be created by breeding. Interestingly, male mdx mice show more severe skeletal muscle disease, while cardiomyopathy is more accurately

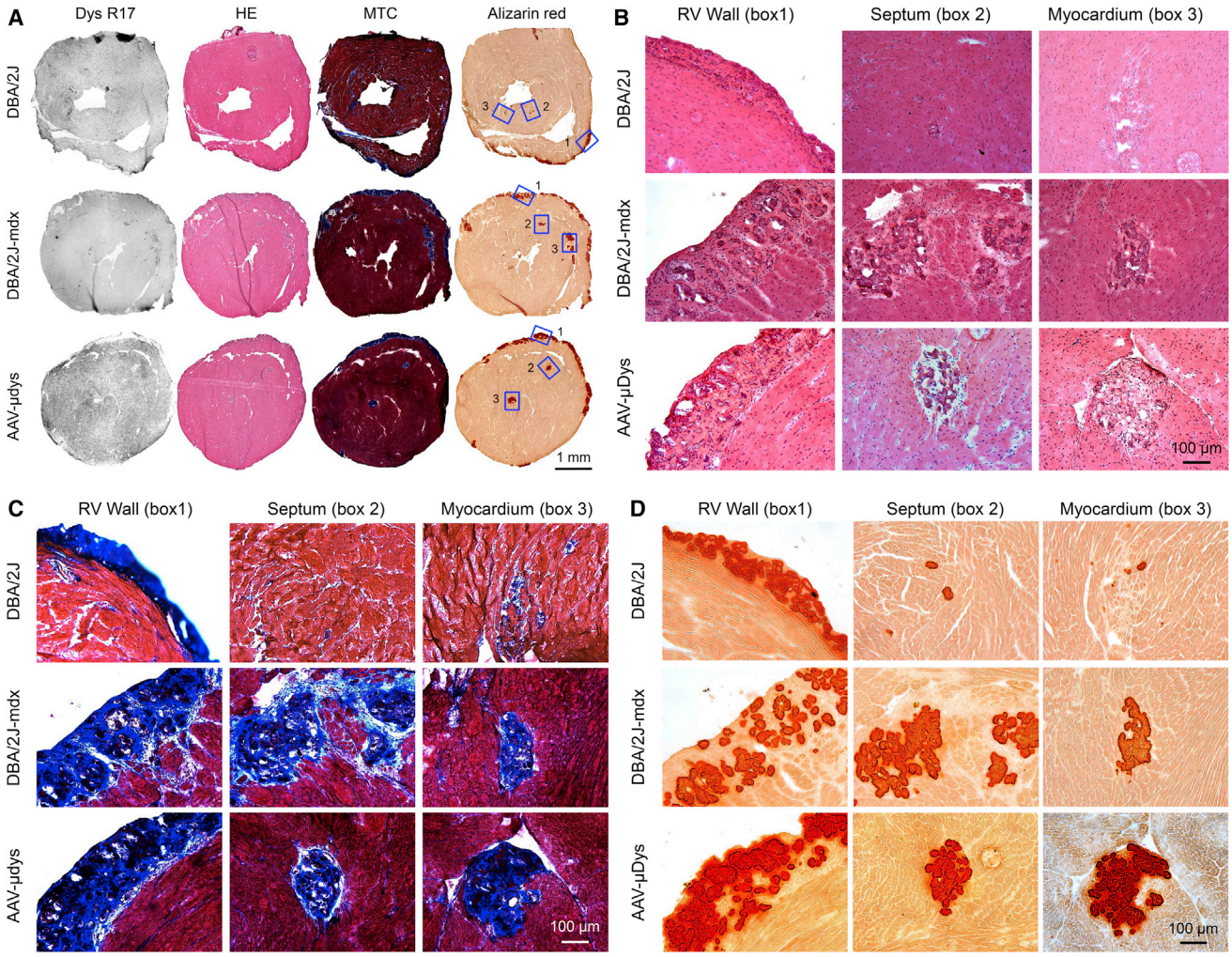

Figure 5. Abnormal Heart Histology in DBA/2J Mice Reveals the Limitation of DBA/2J-mdx Mice as a Model for Studying DMD Heart Disease

(A) Representative full-view photomicrographs of H&E (HE), Masson trichrome (MTC), and alizarin red staining and dystrophin R17 immunostaining of the heart of DBA/2J, untreated, and AAV-treated DBA/2J-mdx mice. Selected areas of interest are numbered with 1, 2, and 3 to represent the right ventricular (RV) wall, septum, and myocardium, respectively. (B) A close view of H&E-stained images of boxed areas 1, 2, and 3 in (A). (C) A close view of Masson trichrome-stained images of boxed areas 1, 2, and 3 in (A). (D) A close view of alizarin red-stained images of boxed areas 1, 2, and 3 in (A).

modeled in female mdx mice.[31,55] Since DBA/2J-mdx mice were suggested to display early-onset heart disease, we included both male and female mice in the study (for the skeletal muscle function assay and cardiac function assay, respectively). We confirmed the severe skeletal muscle phenotype reported in the literature (e.g., fibrosis, calcification, inflammation, relatively poor regeneration, and reduction in muscle force) (Figures 3 and 4; see also Figures S2 and S4).[24,25] AAV micro-dystrophin therapy greatly attenuated (on some occasions, completely normalized) skeletal muscle pathology and restored muscle strength (Figures 3 and 4; see also Figures S2 and S4). Surprisingly, on cardiac evaluation, we were not able to reproduce the published data on the cardiac manifestations of DBA/2J-mdx mice.[24] We observed salient pathological changes in the heart of control DBA/2J mice (both male and female) (Figure 5; see also Figure S5).[24] Cardiac lesions have been observed in DBA/2J mice by several laboratories.[28–30] The existing pathology in control mice rendered it difficult to distinguish additional changes caused by dystrophin deficiency. In fact, we did not detect apparent differences between DBA/2J and DBA/2J-mdx hearts on histological examination (Figure 5; see also Figure S5). Coley et al.[24] found that the maximal cardiac function difference between DBA/2J and DBA/2J-mdx mice occurred at ~6 months of age on echocardiography. The ejection fraction of DBA/2J and DBA/2J-mdx was ~60% and 48%, respectively, at this time point.[24] After which, the heart function of DBA/2J-mdx mice appeared partially recovered although still statistically different from that of DBA/2J mice (the ejection fraction of DBA/2J and DBA/2J-mdx was ~61 and 55, respectively, at 52 weeks of age).[24] We performed our hemodynamic assay at ~6 months of age using the

Table 2. Weights and Weight Ratios

	DBA/2J	DBA/2J-mdx	DBA/2J-mdx Treated
Sample size (n)	10	10	5
Age (months)	6.22 ± 0.15	6.10 ± 0.15	6.12 ± 0.24
BW (g)	25.89 ± 1.25[a]	20.78 ± 0.51	22.48 ± 0.76
TW (mg)	36.68 ± 1.02	30.20 ± 0.72[b]	36.68 ± 0.64
TL (mm)	17.83 ± 0.09	17.84 ± 0.16	17.76 ± 0.08
HW (mg)	110.78 ± 4.32[a]	99.29 ± 2.18	108.74 ± 2.85[c]
VW (mg)	105.41 ± 3.98[a]	94.81 ± 2.09	103.92 ± 2.85[c]
HW/BW (mg/g)	4.30 ± 0.09[b]	4.79 ± 0.07	4.85 ± 0.13
VW/BW (mg/g)	4.10 ± 0.08[b]	4.57 ± 0.07	4.63 ± 0.12
HW/TW (mg/g)	3.02 ± 0.06[a]	3.30 ± 0.09	3.11 ± 0.05
VW/TW (mg/g)	2.87 ± 0.06[a]	3.15 ± 0.08	2.97 ± 0.05
HW/TL (mg/mm)	6.20 ± 0.22[a]	5.56 ± 0.11	6.12 ± 0.14[c]
VW/TL (mg/mm)	5.90 ± 0.20[a]	5.31 ± 0.10	5.85 ± 0.14[c]

Data are presented as means ± SEM.
[a]Significantly different from DBA/2J-mdx.
[b]Significantly different from other two groups.
[c]Significantly different from DBA/2J-mdx on the Mann-Whitney test but not by ANOVA.

cardiac catheter assay (Table 2). Unexpectedly, we did not detect a statistically significant difference in any of the systolic parameters or in most of diastolic parameters between DBA/2J and DBA/2J-mdx mice (Figure 6B). No difference was seen in overall heart function parameters either (e.g., the ejection fraction of DBA/2J and DBA/2J-mdx was 74 ± 4 and 69 ± 4, respectively) (Figure 6B). DMD patients and dystrophic animals display characteristic ECG changes such as tachycardia, reduction in the PR interval, prolongation of the QRS duration and QT interval, a deep Q wave, and an increase in the cardiomyopathy index.[32,34,56–62] However, to our knowledge, ECG has not been examined in DBA/2J-mdx mice. To better understand the heart disease in this model, we compared ECG in DBA/2J, DBA/2J-mdx, and AAV micro-dystrophin treated DBA/2J-mdx mice (Figure 6A; see also Figure S6A). Compared to control DBA/2J mice, untreated DBA/2J-mdx mice showed several features consistent with dystrophin deficiency. Specifically, we detected a statistically significant increase in the QRS duration, QT interval, and cardiomyopathy index. The heart rate was increased but did not reach statistical significance. Intriguingly, a deep Q wave was found in control DBA/2J mice but not in DBA/2J-mdx mice (Figure 6A). In our previous studies, we demonstrated beneficial ECG changes following systemic AAV-9 therapy with a four-repeat micro-dystrophin gene in young and aged mdx mice.[34,53,54] Here, we observed a clear trend of improvement in several ECG parameters but none of them reached statistical significance (Figure 6A). This may be due to the genetic background of the model or the sample size. However, we believe it is not due to a lack of gene transfer, because immunostaining showed saturated expression and western blot analysis suggested a dystrophin level much higher than that of control DBA/2J mice (Figures 1D, 1E, and 5; see also Figure S1B).

In summary, we have provided strong compelling preclinical data in a symptomatic mouse model to support the further development of nNOS-binding five-repeat micro-dystrophin gene therapy for DMD with systemic AAV-9 delivery. The unexpected findings in the heart of control DBA/2J mice reveal the potential limitations of the DBA/2J-mdx model for cardiac studies.

MATERIALS AND METHODS

Animal Studies

All animal experiments were approved by the animal care and use committee of the University of Missouri and were performed in accordance with NIH guidelines. Congenic D2.B10-Dmd^{mdx}/J (stock number 013141; referred to as DBA/2J-mdx in this article) and control DBA/2J (stock number 000671) mice were purchased from The Jackson Laboratory. Experimental mice were generated in house in a barrier facility using founders from The Jackson Laboratory. Both male and female mice were used in the study. Specifically, male mice were used to evaluate skeletal muscle function and female mice were used to study heart function. All mice were maintained in a specific-pathogen free animal care facility on a 12-hr light (25 lux)/12-hr dark cycle with access to food and water ad libitum.

Micro-Dystrophin Construct

The codon-optimized canine microgene ΔR2-15/ΔR18-22/ΔC was based on the human micro-dystrophin cDNA μDys5 (J.R. and J.C., unpublished data) and was synthesized by GenScript. It contains the N-terminal domain, hinges 1 and 4, five spectrin-like repeats (R1, R16, R17, R23, and R24), and the cysteine-rich domain (Figure 1A). The expression cassette was under transcriptional regulation of the muscle-specific CK8 promoter and a 49-bp synthetic pA signal.[1,23,63] The *cis*-AAV packaging plasmid is called pXP42.

AAV Delivery

Recombinant AAV-9 stock was generated at the University of Pennsylvania Vector Core (https://www.med.upenn.edu/gtp/vectorcore) by transient transfection according to the standard protocol of the core. AAV was delivered to 10-week-old DBA/2J-mdx mice through the tail vein in a volume of 500 μL/mouse at the dose of 2×10^{13} vg particles/mouse over a period of 60 s.

AAV Genome Copy Number Quantification

Freshly dissected muscles were snap frozen in liquid nitrogen-cooled isopentane in optimal cutting temperature compound (OCT) (Sakura Finetek). Genomic DNA was extracted from OCT-embedded tissue samples. DNA concentration was quantified with the Qubit dsDNA HS assay kit (Thermo Fisher Scientific). Quantitative TaqMan PCR assays were performed using TaqMan Universal PCR master mix (Thermo Fisher Scientific) to detect either the R1-R16 or R17-R23 junction in the vg. For the R1-R16 junction PCR reaction, the forward primer is 5′ GAGTCGCCTCTATGGAAAAGCA, the reverse primer is 5′ GGTCAGATAAGTACTTGGCACGTAA, and the probe is 5′ ATCTCTTTGTGCAGATTAC. For the R17-R23 junction PCR reaction, the forward primer is 5′ GCCGAACGCAAGAAAAGACT, the reverse primer is 5′ CAGATGGAGCCGCTTCCA, and the probe

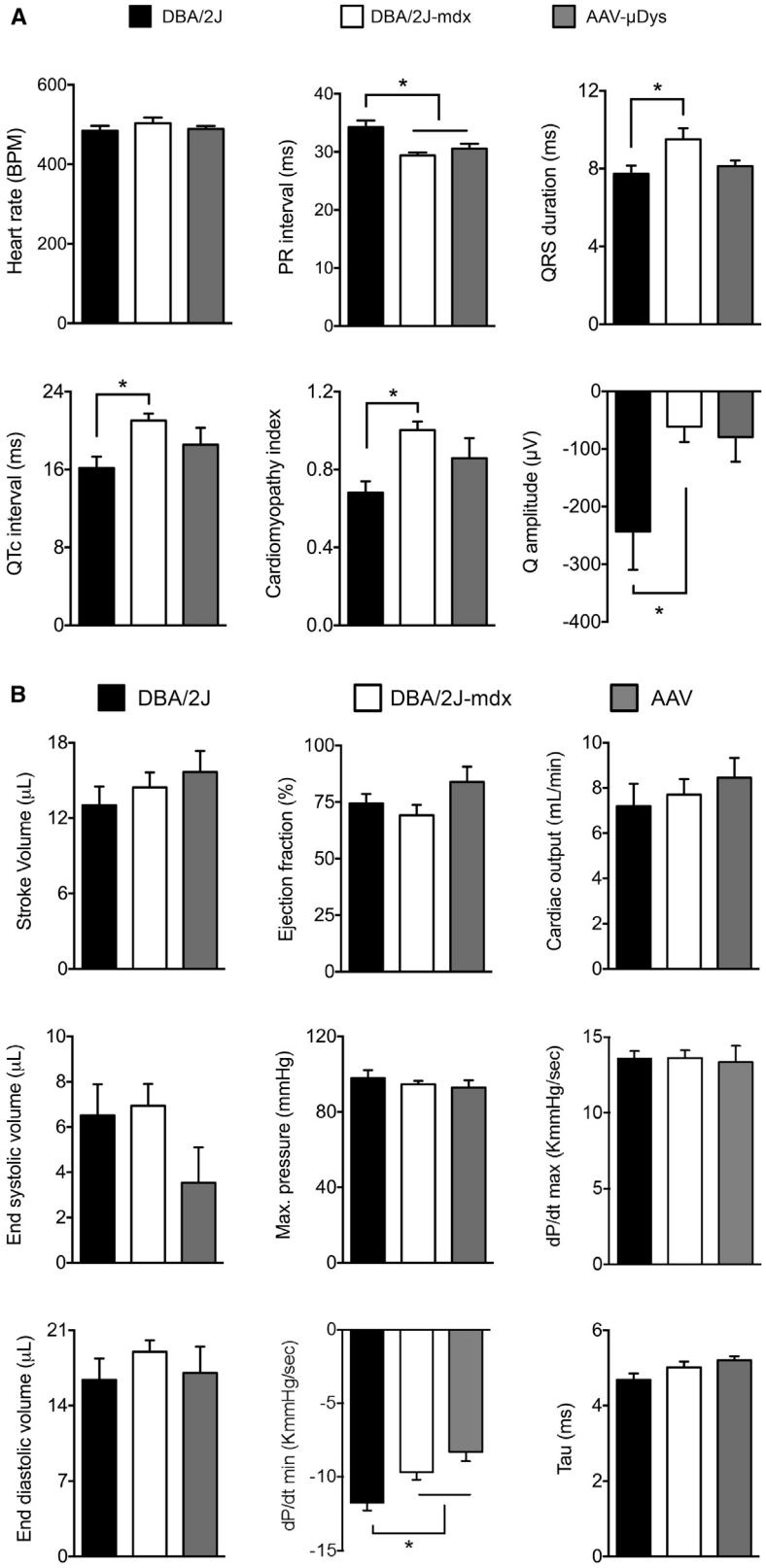

Figure 6. Evaluation of the Cardiac Impact of AAV Micro-Dystrophin Therapy in DBA/2J-mdx Mice

(A) Quantitative evaluation of ECG in DBA/2J (n = 10), untreated (n = 10), and AAV-treated (n = 5) DBA/2J-mdx mice. Error bars are mean ± SEM. Asterisks indicate significant differences from the indicated group(s). (B) Quantitative analysis of systolic function (top panels), diastolic function (middle panels), and overall heart performance (bottom panels). Error bars are mean ± SEM. Asterisks indicate that the result of DBA/2J mice is significantly different from that of AAV-treated DBA/2J-mdx mice.

is 5′ CTGGTCGGAGCTTTCCT. The threshold cycle (Ct) value of each reaction was converted to the vg copy number by measuring against the copy number standard curve of known amount of the pXP42 plasmid. The data are reported as the vg copy number per diploid genome.

Morphological Analysis

Cryosections (10 μm in thickness) were sectioned from OCT-embedded tissue samples and used for staining. General muscle histopathology was revealed with H&E staining. Masson trichrome staining and alizarin red staining were used to reveal muscle fibrosis and myofiber calcification according to our published protocols.[64] Dystrophin expression was evaluated by immunofluorescence staining using two monoclonal antibodies including Mandys-8 (1:200; Sigma) and Manex44A (1:300; a gift from Dr. Glenn Morris, The Robert Jones and Agnes Hunt Orthopaedic Hospital).[65] Mandys-8 recognizes an epitope in dystrophin spectrin-like repeat 11 (R11), which is absent in our micro-dystrophin. Manex44A recognizes an epitope in dystrophin spectrin-like 17 repeat (R17) that is presented in micro-dystrophin. Utrophin was examined with a mouse monoclonal antibody against the utrophin N-terminal domain (VP-U579, 1:20; clone DRP3/20C5, IgG1; Vector Laboratories). β-dystroglycan was revealed with a mouse monoclonal antibody against the C terminus (NCL-b-DG, 1:50; clone 43DAG1/8D5, IgG2a; Novocastra). β-sarcoglycan was revealed with a mouse monoclonal antibody (NCL-b-SARC, 1:50; clone 5B1, IgG1; Novocastra/Leica Biosystems). Dystrobrevin was revealed with a mouse monoclonal antibody (no. 610766, 1:200; clone 23, IgG1; BD Biosciences). Syntrophin was revealed with a pan-syntrophin mouse monoclonal antibody (ab11425, 1:200; clone 1351, IgG1; Abcam). In situ nNOS activity staining was performed according to a published protocol.[18] Macrophages and neutrophils were detected by immunohistochemical staining with the rat anti-mouse F4/80 antibody (1:200; Caltag Laboratories) and the rat anti-mouse Ly-6G antibody (1:800; BD Biosciences PharMingen), respectively. Slides were viewed at the identical exposure setting using a Nikon E800 fluorescence microscope. Photomicrographs were taken with a QImage Retiga 1300 camera (QImaging).

Central nucleation and the myofiber size were determined from digitalized H&E-stained images using Fiji imaging software (https://fiji.sc).[66] The myofiber size was determined using Feret's minimum diameter method.

Western Blot Analysis

Freshly dissected muscle tissues were snap frozen in liquid nitrogen. Muscle was then homogenized using a liquid nitrogen-cooled mortar and pestle in a homogenization buffer containing 10% SDS, 5 mM ethylenediaminetetraacetic acid, 62.5 mM Tris-HCl (pH 6.8), and 2% protease inhibitor (Roche). Homogenate was spun at 14,000 rpm for 2 min (Eppendorf centrifuge, model 5417C; Eppendorf-Netheler-Hinz). The supernatant was used for western blot analysis. Protein concentration was determined using the Bio-Rad DC protein assay kit (Bio-Rad). 100–150 μg protein was loaded on a 3% stacking/6% separating SDS-polyacrylamide gel and run for 3.5 hr at 100 V. Following electrophoresis, protein was transferred to a polyvinylidene fluoride (PVDF) membrane. The PVDF membrane was blocked with 5% milk in Tris-buffered saline (TBS)-Tween 20 (TBST) solution (containing 1× TBS and 0.1% Tween 20) for 1 hr at room temperature. The PVDF membrane was subsequently incubated with a dystrophin monoclonal antibody MANHINGE1A (1:100 dilution; a gift from Dr. Glenn Morris) in 5% milk/TBST overnight at 4°C. The membrane was washed in TBST three times for 10 min each and then incubated with the horseradish peroxidase-conjugated goat anti-mouse IgG secondary antibody (1:2,000 dilution in TBST; Santa Cruz) for 1 hr at room temperature. After another round of TBST wash (three times, 10-min each), signals were detected using the enhanced chemiluminescence (ECL) system (GE Healthcare Biosciences). Protein loading was confirmed with Ponceau S staining.

Skeletal Muscle Function Assay

Function of the EDL muscle and the TA muscle was evaluated ex vivo and in situ, respectively, according to our published protocols.[67,68] Specifically, the twitch force, tetanic force, and eccentric contraction profile were measured. Experimental mice were anesthetized via intraperitoneal injection of a cocktail containing 25 mg/mL ketamine, 2.5 mg/mL xylazine, and 0.5 mg/mL acepromazine at 2.5 μL/g body weight. For the ex vivo EDL muscle function assay, the muscle was gently dissected and mounted to a muscle test system (Aurora Scientific). Muscle force was evaluated with a 305B dual-mode servomotor transducer (Aurora Scientific). For the in situ TA muscle function assay, the TA muscle and the sciatic nerve were exposed. The mouse was then transferred to a custom-designed thermo-controlled footplate platform.[67] Subsequently, forces were measured in situ with a 305C-LR dual-mode servomotor transducer (Aurora Scientific). Data acquisition and analysis was performed with Dynamic Muscle Control and Analysis software (Aurora Scientific). The specific muscle force was calculated by dividing the absolute muscle force by the muscle cross-sectional area. Muscle CSA was calculated according to the following equation: CSA = (muscle mass, in g)/[(muscle density, in g/cm^3) × (length ratio) × (optimal muscle length, in cm)]; 1.06 g/cm^3 was used for muscle density.[69] The length ratio refers to the ratio of the optimal fiber length to the optimal muscle length. The length ratios for the EDL and TA muscles were 0.44 and 0.6, respectively.[70,71]

Heart Function Assay

A 12-lead ECG assay was performed using a commercial system from AD Instruments according to our previously published protocol.[72,73] The Q wave amplitude was determined using the lead I tracing. Other ECG parameters were analyzed using the lead II tracing. The QTc interval was determined by correcting the QT interval with the heart rate, as described by Mitchell et al.[74] The cardiomyopathy index was calculated by dividing the QT interval by the PQ segment.[75] Left ventricular hemodynamics was evaluated using a Millar ultra-miniature pressure-volume (PV) catheter SPR 839. The catheter was placed in the left ventricle using a closed chest approach as we previously described.[72,73] The resulting PV loops were analyzed with PVAN software (Millar Instruments). The relaxation constant of the left ventricle was determined using the method of Weiss

et al.[76] Detailed protocols for ECG and hemodynamic assays are available at the Parent Project Muscular Dystrophy standard operating protocol website (http://www.parentprojectmd.org/site/PageServer?pagename=Advance_researchers_sops).[77]

Statistical Analysis

Data are presented as means ± SEM. Statistical significance was determined with one-way ANOVA followed by Tukey multiple comparison analysis or Bonferroni post hoc analysis using GraphPad Prism software (version 7.0) or SPSS statistical software (IBM). For data that did not fit into the Gaussian distribution, the nonparametric Mann-Whitney test was used to evaluate the statistical significance in two-group comparisons. The difference was considered significant when $p < 0.05$.

SUPPLEMENTAL INFORMATION

Supplemental Information includes six figures and can be found with this article online at http://dx.doi.org/10.1016/j.omtm.2017.06.006.

AUTHOR CONTRIBUTIONS

Conceived and designed experiments: C.H.H., N.B.W., J.S.S., J.S.C., and D.D. Performed the experiments: C.H.H., N.B.W., X.P., K.K., Y.Y., K.Z., G.Y., B.H., S.X.D., and J.R. Analyzed the data: C.H.H., N.B.W., J.S.S., N.N.Y., J.S.C., and D.D. Wrote the paper: C.H.H., N.B.W., and D.D. All authors edited the paper and approved the submission.

CONFLICTS OF INTEREST

D.D. and J.S.C. are members of the scientific advisory board and are equity holders of Solid Biosciences, LLC. D.D., J.R., J.S.C., and Y.Y. are inventors on patents that were licensed to Solid Biosciences, LLC. The Duan laboratory and the Chamberlain laboratory have received research support from Solid Biosciences, LLC. J.S.S. is an employee of Solid Biosciences, LLC.

ACKNOWLEDGMENTS

This work was supported in part by Solid Biosciences, LLC and by grants from the NIH (NS-90634 to D.D. and HL-122332 to J.S.C.), the Department of Defense (MD130014 to D.D.), Jesse's Journey–The Foundation for Gene and Cell Therapy (to D.D.), and the Jackson Freel DMD Research Fund (to D.D.). We thank Dr. Patrick Gonzalez for the critical reading of the manuscript. We thank Dr. Stephen Hauschka for providing the CK8 promoter.

REFERENCES

1. Bengtsson, N.E., Seto, J.T., Hall, J.K., Chamberlain, J.S., and Odom, G.L. (2016). Progress and prospects of gene therapy clinical trials for the muscular dystrophies. Hum. Mol. Genet. *25*, R9–R17.
2. Duan, D. (2016). Dystrophin gene replacement and gene repair therapy for Duchenne muscular dystrophy in 2016. Hum. Gene Ther. Clin. Dev. *27*, 9–18.
3. Al-Zaidy, S., Rodino-Klapac, L., and Mendell, J.R. (2014). Gene therapy for muscular dystrophy: moving the field forward. Pediatr. Neurol. *51*, 607–618.
4. Duan, D. (2016). Systemic delivery of adeno-associated viral vectors. Curr. Opin. Virol. *21*, 16–25.
5. Mingozzi, F., and High, K.A. (2011). Therapeutic in vivo gene transfer for genetic disease using AAV: progress and challenges. Nat. Rev. Genet. *12*, 341–355.
6. Mendell, J.R., Al-Zaidy, S., Shell, R., Arnold, W.D., Rodino-Klapac, L., Kissel, J.T., Prior, T.W., Miranda, C., Lowes, L., Alfano, L., and Berry, K. (2016). Gene therapy for spinal muscular atrophy type 1 shows potential to improve survival and motor functional outcomes. Mol. Ther. *24*, S190.
7. Carter, B.J. (2004). Adeno-associated virus and the development of adeno-associated virus vectors: a historical perspective. Mol. Ther. *10*, 981–989.
8. England, S.B., Nicholson, L.V., Johnson, M.A., Forrest, S.M., Love, D.R., Zubrzycka-Gaarn, E.E., Bulman, D.E., Harris, J.B., and Davies, K.E. (1990). Very mild muscular dystrophy associated with the deletion of 46% of dystrophin. Nature *343*, 180–182.
9. Crawford, G.E., Faulkner, J.A., Crosbie, R.H., Campbell, K.P., Froehner, S.C., and Chamberlain, J.S. (2000). Assembly of the dystrophin-associated protein complex does not require the dystrophin COOH-terminal domain. J. Cell Biol. *150*, 1399–1410.
10. Wang, B., Li, J., and Xiao, X. (2000). Adeno-associated virus vector carrying human minidystrophin genes effectively ameliorates muscular dystrophy in mdx mouse model. Proc. Natl. Acad. Sci. USA *97*, 13714–13719.
11. Harper, S.Q., Hauser, M.A., DelloRusso, C., Duan, D., Crawford, R.W., Phelps, S.F., Harper, H.A., Robinson, A.S., Engelhardt, J.F., Brooks, S.V., and Chamberlain, J.S. (2002). Modular flexibility of dystrophin: implications for gene therapy of Duchenne muscular dystrophy. Nat. Med. *8*, 253–261.
12. Liu, M., Yue, Y., Harper, S.Q., Grange, R.W., Chamberlain, J.S., and Duan, D. (2005). Adeno-associated virus-mediated microdystrophin expression protects young mdx muscle from contraction-induced injury. Mol. Ther. *11*, 245–256.
13. Gregorevic, P., Allen, J.M., Minami, E., Blankinship, M.J., Haraguchi, M., Meuse, L., Finn, E., Adams, M.E., Froehner, S.C., Murry, C.E., and Chamberlain, J.S. (2006). rAAV6-microdystrophin preserves muscle function and extends lifespan in severely dystrophic mice. Nat. Med. *12*, 787–789.
14. Wang, B., Li, J., Fu, F.H., and Xiao, X. (2009). Systemic human minidystrophin gene transfer improves functions and life span of dystrophin and dystrophin/utrophin-deficient mice. J. Orthop. Res. *27*, 421–426.
15. Yue, Y., Liu, M., and Duan, D. (2006). C-terminal-truncated microdystrophin recruits dystrobrevin and syntrophin to the dystrophin-associated glycoprotein complex and reduces muscular dystrophy in symptomatic utrophin/dystrophin double-knockout mice. Mol. Ther. *14*, 79–87.
16. Brenman, J.E., Chao, D.S., Xia, H., Aldape, K., and Bredt, D.S. (1995). Nitric oxide synthase complexed with dystrophin and absent from skeletal muscle sarcolemma in Duchenne muscular dystrophy. Cell *82*, 743–752.
17. Li, D., Yue, Y., Lai, Y., Hakim, C.H., and Duan, D. (2011). Nitrosative stress elicited by nNOSμ delocalization inhibits muscle force in dystrophin-null mice. J. Pathol. *223*, 88–98.
18. Lai, Y., Thomas, G.D., Yue, Y., Yang, H.T., Li, D., Long, C., Judge, L., Bostick, B., Chamberlain, J.S., Terjung, R.L., and Duan, D. (2009). Dystrophins carrying spectrin-like repeats 16 and 17 anchor nNOS to the sarcolemma and enhance exercise performance in a mouse model of muscular dystrophy. J. Clin. Invest. *119*, 624–635.
19. Lai, Y., Zhao, J., Yue, Y., and Duan, D. (2013). α2 and α3 helices of dystrophin R16 and R17 frame a microdomain in the α1 helix of dystrophin R17 for neuronal NOS binding. Proc. Natl. Acad. Sci. USA *110*, 525–530.
20. Zhang, Y., and Duan, D. (2012). Novel mini-dystrophin gene dual adeno-associated virus vectors restore neuronal nitric oxide synthase expression at the sarcolemma. Hum. Gene Ther. *23*, 98–103.
21. Zhang, Y., Yue, Y., Li, L., Hakim, C.H., Zhang, K., Thomas, G.D., and Duan, D. (2013). Dual AAV therapy ameliorates exercise-induced muscle injury and functional ischemia in murine models of Duchenne muscular dystrophy. Hum. Mol. Genet. *22*, 3720–3729.
22. Shin, J.H., Pan, X., Hakim, C.H., Yang, H.T., Yue, Y., Zhang, K., Terjung, R.L., and Duan, D. (2013). Microdystrophin ameliorates muscular dystrophy in the canine model of duchenne muscular dystrophy. Mol. Ther. *21*, 750–757.
23. Himeda, C.L., Chen, X., and Hauschka, S.D. (2011). Design and testing of regulatory cassettes for optimal activity in skeletal and cardiac muscles. Methods Mol. Biol. *709*, 3–19.

24. Coley, W.D., Bogdanik, L., Vila, M.C., Yu, Q., Van Der Meulen, J.H., Rayavarapu, S., Novak, J.S., Nearing, M., Quinn, J.L., Saunders, A., et al. (2016). Effect of genetic background on the dystrophic phenotype in mdx mice. Hum. Mol. Genet. *25*, 130–145.

25. Fukada, S., Morikawa, D., Yamamoto, Y., Yoshida, T., Sumie, N., Yamaguchi, M., Ito, T., Miyagoe-Suzuki, Y., Takeda, S., Tsujikawa, K., and Yamamoto, H. (2010). Genetic background affects properties of satellite cells and mdx phenotypes. Am. J. Pathol. *176*, 2414–2424.

26. Wasala, N.B., Zhang, K., Wasala, L.P., Hakim, C.H., and Duan, D. (2015). The FVB background does not dramatically alter the dystrophic phenotype of mdx mice. PLoS Curr., Published online February 10, 2015. http://dx.doi.org/10.1371/currents.md.28266819ca0ec5fefcac767ea9a3461c.

27. Li, D., Yue, Y., and Duan, D. (2008). Preservation of muscle force in Mdx3cv mice correlates with low-level expression of a near full-length dystrophin protein. Am. J. Pathol. *172*, 1332–1341.

28. Maeda, N., Doi, K., and Mitsuoka, T. (1986). Development of heart and aortic lesions in DBA/2NCrj mice. Lab. Anim. *20*, 5–8.

29. Brownstein, D.G. (1983). Genetics of dystrophic epicardial mineralization in DBA/2 mice. Lab. Anim. Sci. *33*, 247–248.

30. Nabors, C.E., and Ball, C.R. (1969). Spontaneous calcification in hearts of DBA mice. Anat. Rec. *164*, 153–161.

31. Bostick, B., Yue, Y., and Duan, D. (2010). Gender influences cardiac function in the mdx model of Duchenne cardiomyopathy. Muscle Nerve *42*, 600–603.

32. Bostick, B., Yue, Y., Long, C., and Duan, D. (2008). Prevention of dystrophin-deficient cardiomyopathy in twenty-one-month-old carrier mice by mosaic dystrophin expression or complementary dystrophin/utrophin expression. Circ. Res. *102*, 121–130.

33. Yue, Y., Wasala, N.B., Bostick, B., and Duan, D. (2016). 100-fold but not 50-fold dystrophin overexpression aggravates electrocardiographic defects in the mdx model of Duchenne muscular dystrophy. Mol. Ther. Methods Clin. Dev. *3*, 16045.

34. Bostick, B., Yue, Y., Lai, Y., Long, C., Li, D., and Duan, D. (2008). Adeno-associated virus serotype-9 microdystrophin gene therapy ameliorates electrocardiographic abnormalities in mdx mice. Hum. Gene Ther. *19*, 851–856.

35. Lai, Y., Yue, Y., Liu, M., Ghosh, A., Engelhardt, J.F., Chamberlain, J.S., and Duan, D. (2005). Efficient in vivo gene expression by trans-splicing adeno-associated viral vectors. Nat. Biotechnol. *23*, 1435–1439.

36. Ghosh, A., Yue, Y., Lai, Y., and Duan, D. (2008). A hybrid vector system expands adeno-associated viral vector packaging capacity in a transgene-independent manner. Mol. Ther. *16*, 124–130.

37. Lostal, W., Kodippili, K., Yue, Y., and Duan, D. (2014). Full-length dystrophin reconstitution with adeno-associated viral vectors. Hum. Gene Ther. *25*, 552–562.

38. Odom, G.L., Gregorevic, P., Allen, J.M., and Chamberlain, J.S. (2011). Gene therapy of mdx mice with large truncated dystrophins generated by recombination using rAAV6. Mol. Ther. *19*, 36–45.

39. Koo, T., Popplewell, L., Athanasopoulos, T., and Dickson, G. (2014). Triple trans-splicing adeno-associated virus vectors capable of transferring the coding sequence for full-length dystrophin protein into dystrophic mice. Hum. Gene Ther. *25*, 98–108.

40. Mendell, J.R., Campbell, K., Rodino-Klapac, L., Sahenk, Z., Shilling, C., Lewis, S., Bowles, D., Gray, S., Li, C., Galloway, G., et al. (2010). Dystrophin immunity in Duchenne's muscular dystrophy. N. Engl. J. Med. *363*, 1429–1437.

41. Gregorevic, P., Blankinship, M.J., Allen, J.M., Crawford, R.W., Meuse, L., Miller, D.G., Russell, D.W., and Chamberlain, J.S. (2004). Systemic delivery of genes to striated muscles using adeno-associated viral vectors. Nat. Med. *10*, 828–834.

42. Yue, Y., Pan, X., Hakim, C.H., Kodippili, K., Zhang, K., Shin, J.H., Yang, H.T., McDonald, T., and Duan, D. (2015). Safe and bodywide muscle transduction in young adult Duchenne muscular dystrophy dogs with adeno-associated virus. Hum. Mol. Genet. *24*, 5880–5890.

43. Baroncelli, A.B., Abellonio, F., Pagano, T.B., Esposito, I., Peirone, B., Papparella, S., and Paciello, O. (2014). Muscular dystrophy in a dog resembling human Becker muscular dystrophy. J. Comp. Pathol. *150*, 429–433.

44. Stamler, J.S., and Meissner, G. (2001). Physiology of nitric oxide in skeletal muscle. Physiol. Rev. *81*, 209–237.

45. De Palma, C., and Clementi, E. (2012). Nitric oxide in myogenesis and therapeutic muscle repair. Mol. Neurobiol. *46*, 682–692.

46. Thomas, G.D. (2013). Functional muscle ischemia in Duchenne and Becker muscular dystrophy. Front. Physiol. *4*, 381.

47. Tidball, J.G., and Wehling-Henricks, M. (2014). Nitric oxide synthase deficiency and the pathophysiology of muscular dystrophy. J. Physiol. *592*, 4627–4638.

48. Wang, Z., Kuhr, C.S., Allen, J.M., Blankinship, M., Gregorevic, P., Chamberlain, J.S., Tapscott, S.J., and Storb, R. (2007). Sustained AAV-mediated dystrophin expression in a canine model of Duchenne muscular dystrophy with a brief course of immunosuppression. Mol. Ther. *15*, 1160–1166.

49. Gao, G., Vandenberghe, L.H., Alvira, M.R., Lu, Y., Calcedo, R., Zhou, X., and Wilson, J.M. (2004). Clades of Adeno-associated viruses are widely disseminated in human tissues. J. Virol. *78*, 6381–6388.

50. Bostick, B., Ghosh, A., Yue, Y., Long, C., and Duan, D. (2007). Systemic AAV-9 transduction in mice is influenced by animal age but not by the route of administration. Gene Ther. *14*, 1605–1609.

51. Yue, Y., Ghosh, A., Long, C., Bostick, B., Smith, B.F., Kornegay, J.N., and Duan, D. (2008). A single intravenous injection of adeno-associated virus serotype-9 leads to whole body skeletal muscle transduction in dogs. Mol. Ther. *16*, 1944–1952.

52. Yue, Y., Shin, J.H., and Duan, D. (2011). Whole body skeletal muscle transduction in neonatal dogs with AAV-9. Methods Mol. Biol. *709*, 313–329.

53. Bostick, B., Shin, J.-H., Yue, Y., and Duan, D. (2011). AAV-microdystrophin therapy improves cardiac performance in aged female mdx mice. Mol. Ther. *19*, 1826–1832.

54. Bostick, B., Shin, J.H., Yue, Y., Wasala, N.B., Lai, Y., and Duan, D. (2012). AAV micro-dystrophin gene therapy alleviates stress-induced cardiac death but not myocardial fibrosis in >21-m-old mdx mice, an end-stage model of Duchenne muscular dystrophy cardiomyopathy. J. Mol. Cell. Cardiol. *53*, 217–222.

55. Hakim, C.H., and Duan, D. (2012). Gender differences in contractile and passive properties of mdx extensor digitorum longus muscle. Muscle Nerve *45*, 250–256.

56. Shin, J.H., Bostick, B., Yue, Y., Hajjar, R., and Duan, D. (2011). SERCA2a gene transfer improves electrocardiographic performance in aged mdx mice. J. Transl. Med. *9*, 132.

57. Fine, D.M., Shin, J.H., Yue, Y., Volkmann, D., Leach, S.B., Smith, B.F., McIntosh, M., and Duan, D. (2011). Age-matched comparison reveals early electrocardiography and echocardiography changes in dystrophin-deficient dogs. Neuromuscul. Disord. *21*, 453–461.

58. Perloff, J.K., Roberts, W.C., de Leon, A.C., Jr., and O'Doherty, D. (1967). The distinctive electrocardiogram of Duchenne's progressive muscular dystrophy. An electrocardiographic-pathologic correlative study. Am. J. Med. *42*, 179–188.

59. Perloff, J.K. (1984). Cardiac rhythm and conduction in Duchenne's muscular dystrophy: a prospective study of 20 patients. J. Am. Coll. Cardiol. *3*, 1263–1268.

60. Fayssoil, A. (2008). Holter electrocardiogram should be systematic in Duchenne muscular dystrophy. Int. J. Cardiol. *128*, 442–443.

61. Takami, Y., Takeshima, Y., Awano, H., Okizuka, Y., Yagi, M., and Matsuo, M. (2008). High incidence of electrocardiogram abnormalities in young patients with Duchenne muscular dystrophy. Pediatr. Neurol. *39*, 399–403.

62. Thrush, P.T., Allen, H.D., Viollet, L., and Mendell, J.R. (2009). Re-examination of the electrocardiogram in boys with Duchenne muscular dystrophy and correlation with its dilated cardiomyopathy. Am. J. Cardiol. *103*, 262–265.

63. Levitt, N., Briggs, D., Gil, A., and Proudfoot, N.J. (1989). Definition of an efficient synthetic poly(A) site. Genes Dev. *3*, 1019–1025.

64. Smith, B.F., Yue, Y., Woods, P.R., Kornegay, J.N., Shin, J.H., Williams, R.R., and Duan, D. (2011). An intronic LINE-1 element insertion in the dystrophin gene aborts dystrophin expression and results in Duchenne-like muscular dystrophy in the corgi breed. Lab. Invest. *91*, 216–231.

65. Kodippili, K., Vince, L., Shin, J.H., Yue, Y., Morris, G.E., McIntosh, M.A., and Duan, D. (2014). Characterization of 65 epitope-specific dystrophin monoclonal antibodies in canine and murine models of duchenne muscular dystrophy by immunostaining and western blot. PLoS ONE *9*, e88280.

66. Schindelin, J., Arganda-Carreras, I., Frise, E., Kaynig, V., Longair, M., Pietzsch, T., Preibisch, S., Rueden, C., Saalfeld, S., Schmid, B., et al. (2012). Fiji: an open-source platform for biological-image analysis. Nat. Methods *9*, 676–682.

67. Hakim, C.H., Wasala, N.B., and Duan, D. (2013). Evaluation of muscle function of the extensor digitorum longus muscle ex vivo and tibialis anterior muscle in situ in mice. J. Vis. Exp. *72*, 50183.

68. Hakim, C.H., Li, D., and Duan, D. (2011). Monitoring murine skeletal muscle function for muscle gene therapy. Methods Mol. Biol. *709*, 75–89.

69. Mendez, J., and Keys, A. (1960). Density and composition of mammalian muscle. Metabolism *9*, 184–188.

70. Burkholder, T.J., Fingado, B., Baron, S., and Lieber, R.L. (1994). Relationship between muscle fiber types and sizes and muscle architectural properties in the mouse hindlimb. J. Morphol. *221*, 177–190.

71. Brooks, S.V., and Faulkner, J.A. (1988). Contractile properties of skeletal muscles from young, adult and aged mice. J. Physiol. *404*, 71–82.

72. Bostick, B., Yue, Y., and Duan, D. (2011). Phenotyping cardiac gene therapy in mice. Methods Mol. Biol. *709*, 91–104.

73. Wasala, N.B., Bostick, B., Yue, Y., and Duan, D. (2013). Exclusive skeletal muscle correction does not modulate dystrophic heart disease in the aged mdx model of Duchenne cardiomyopathy. Hum. Mol. Genet. *22*, 2634–2641.

74. Mitchell, G.F., Jeron, A., and Koren, G. (1998). Measurement of heart rate and Q-T interval in the conscious mouse. Am. J. Physiol. *274*, H747–H751.

75. Nigro, G., Comi, L.I., Politano, L., and Nigro, G. (2004). Cardiomyopathies associated with muscular dystrophies. In Myology: Basic and Clinical, Third Edition, *Volume 2*, A. Engel and C. Franzini-Armstrong, eds. (McGraw-Hill, Medical Publishing Division), pp. 1239–1256.

76. Weiss, J.L., Frederiksen, J.W., and Weisfeldt, M.L. (1976). Hemodynamic determinants of the time-course of fall in canine left ventricular pressure. J. Clin. Invest. *58*, 751–760.

77. Duan, D., Rafael-Fortney, J.A., Blain, A., Kass, D.A., McNally, E.M., Metzger, J.M., Spurney, C.F., and Kinnett, K. (2016). Standard operating procedures (SOPs) for evaluating the heart in preclinical studies of Duchenne muscular dystrophy. J. Cardiovasc. Transl. Res. *9*, 85–86.

OMTM, Volume *6*

Supplemental Information

A Five-Repeat Micro-Dystrophin Gene Ameliorated Dystrophic Phenotype in the Severe DBA/2J-mdx Model of Duchenne Muscular Dystrophy

Chady H. Hakim, Nalinda B. Wasala, Xiufang Pan, Kasun Kodippili, Yongping Yue, Keqing Zhang, Gang Yao, Brittney Haffner, Sean X. Duan, Julian Ramos, Joel S. Schneider, N. Nora Yang, Jeffrey S. Chamberlain, and Dongsheng Duan

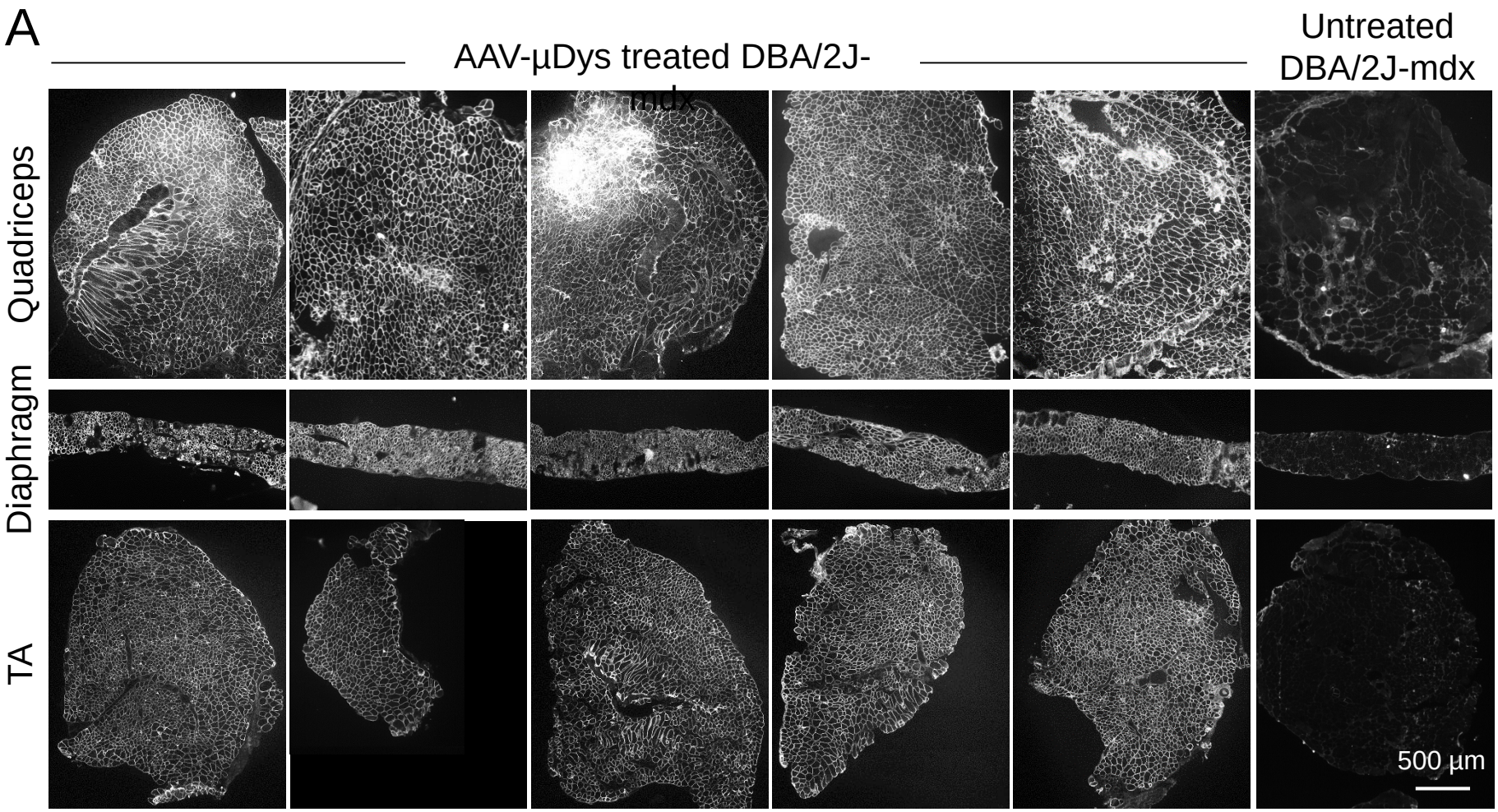
A
AAV-µDys treated DBA/2J-mdx
Untreated DBA/2J-mdx
Quadriceps
Diaphragm
TA
500 µm

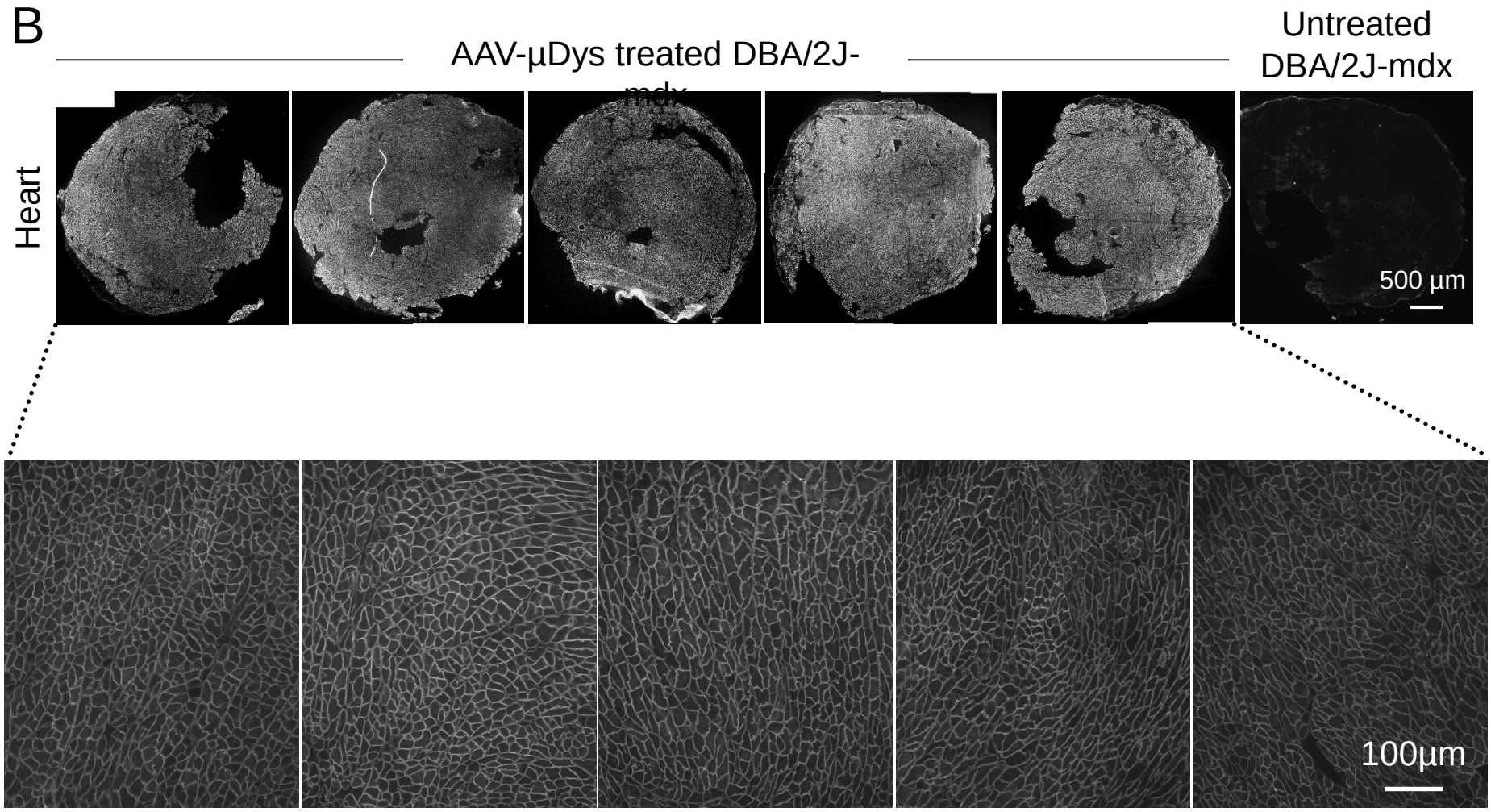
B
AAV-µDys treated DBA/2J-mdx
Untreated DBA/2J-mdx
Heart
500 µm
100µm

Hakim et al. 2017 Figure S1C

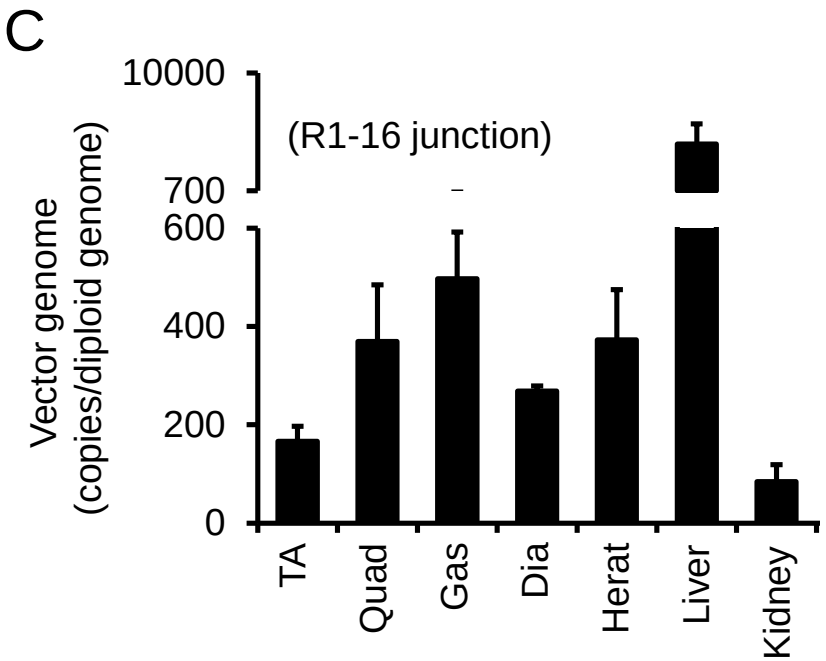

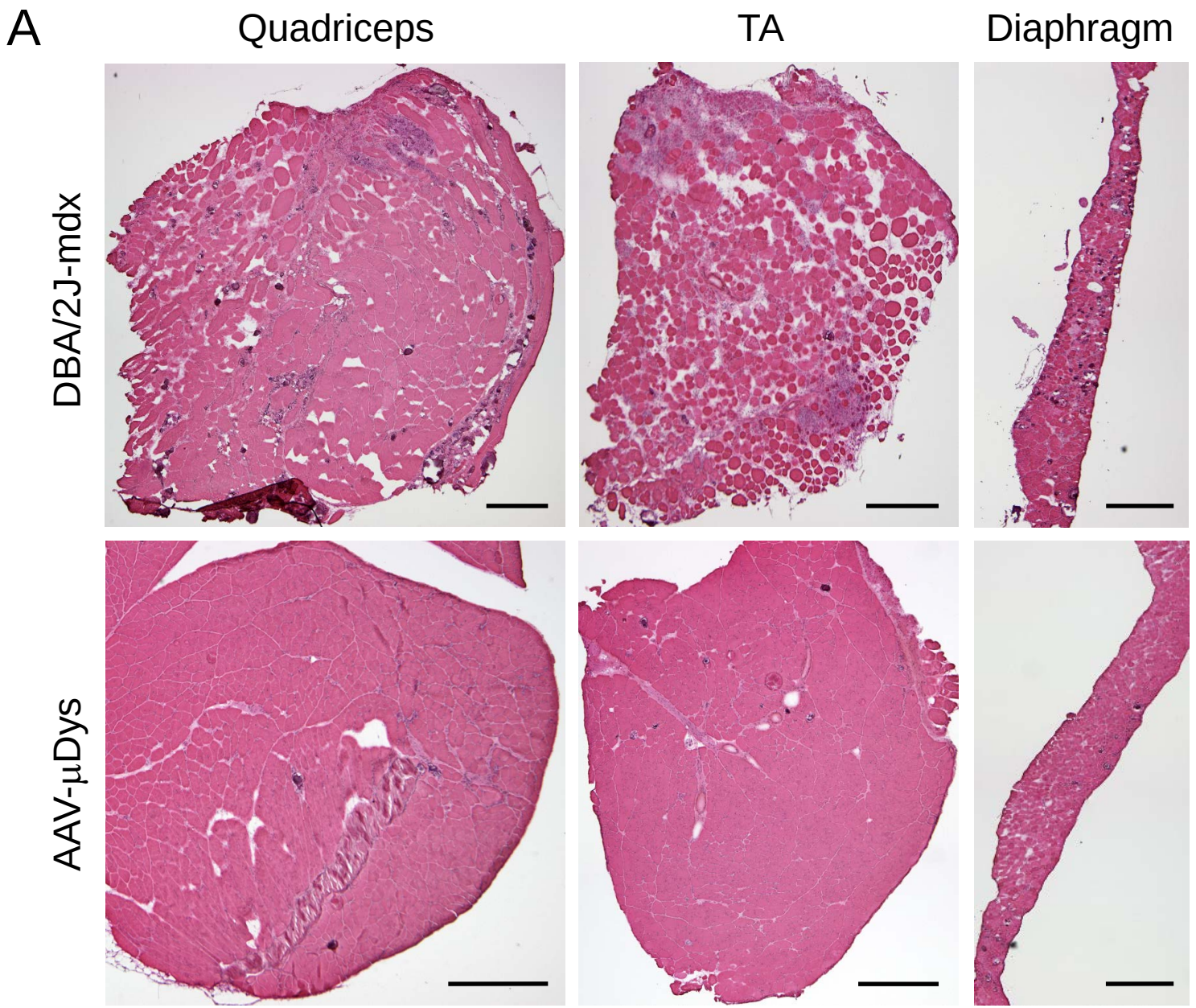
A
Quadriceps
TA
Diaphragm
DBA/2J-mdx
AAV-μDys

Hakim et al. 2017 Figure S2B

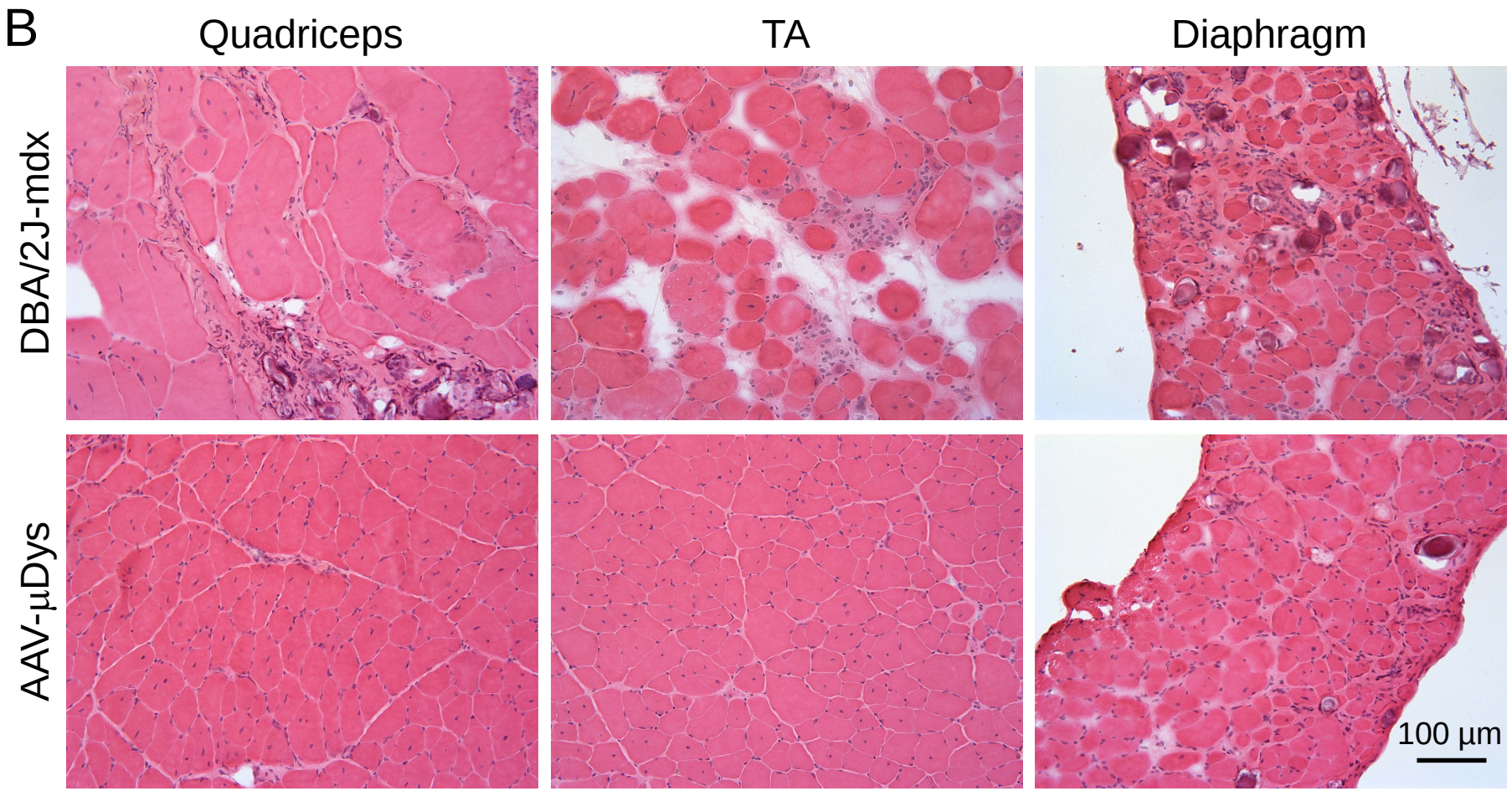

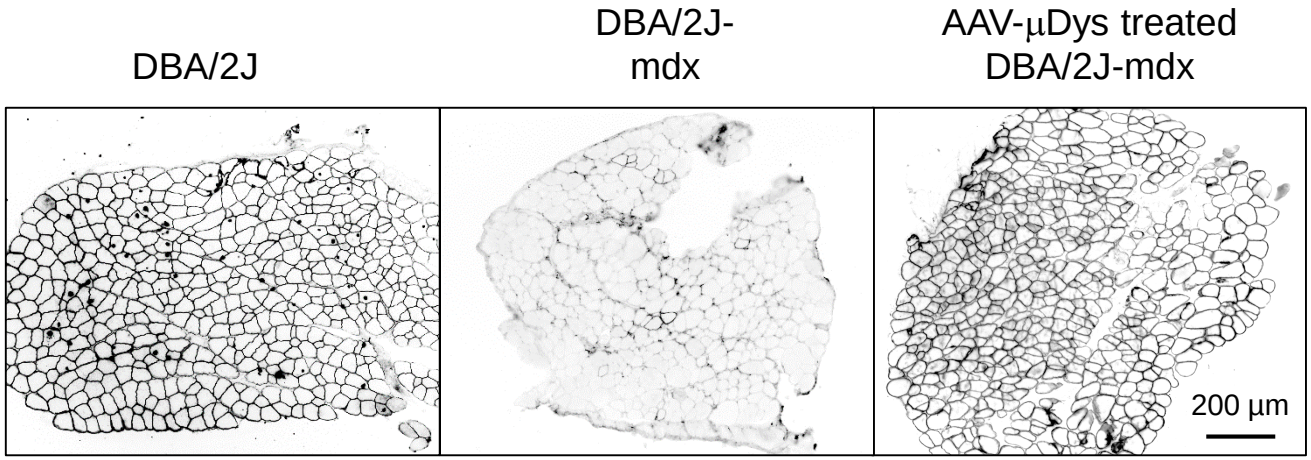
DBA/2J
DBA/2J-mdx
AAV-μDys treated DBA/2J-mdx
200 μm

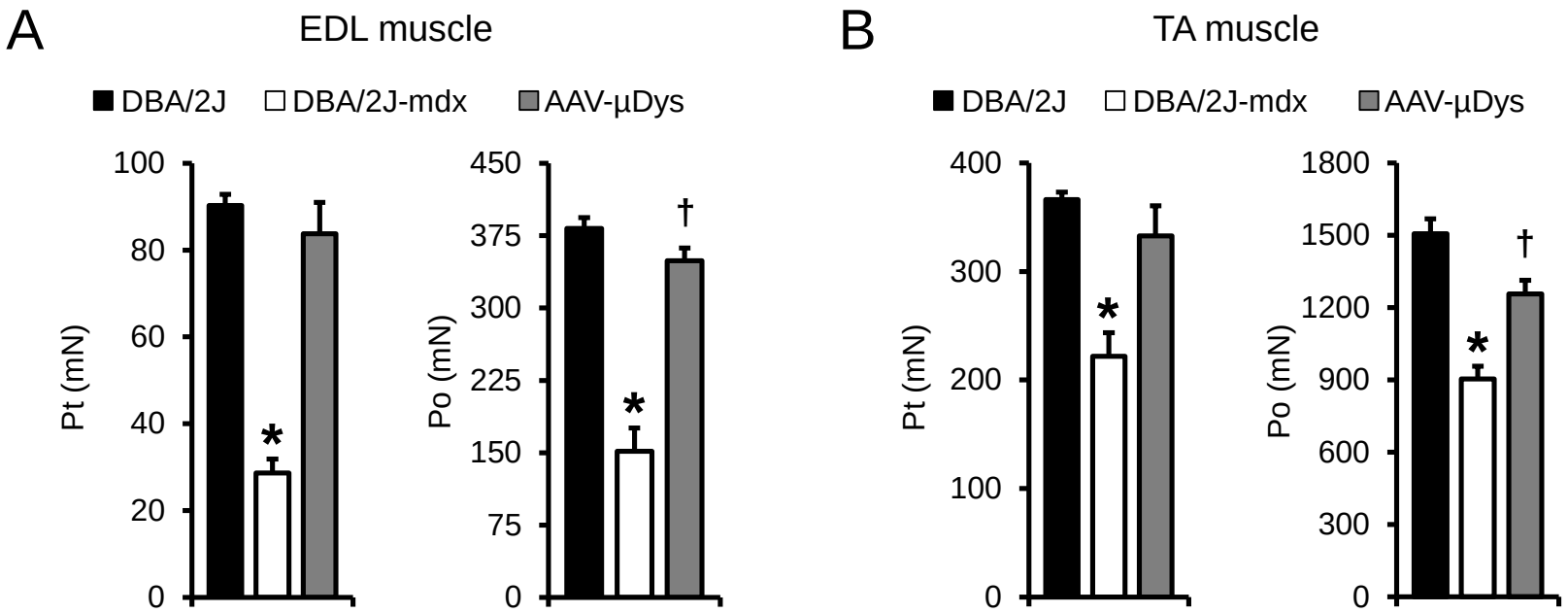

*, DBA/mdx is significant different from DBA and AAV treated
†, DBA is significant different from treated AAV treated

Hakim et al. 2017 Figure S5

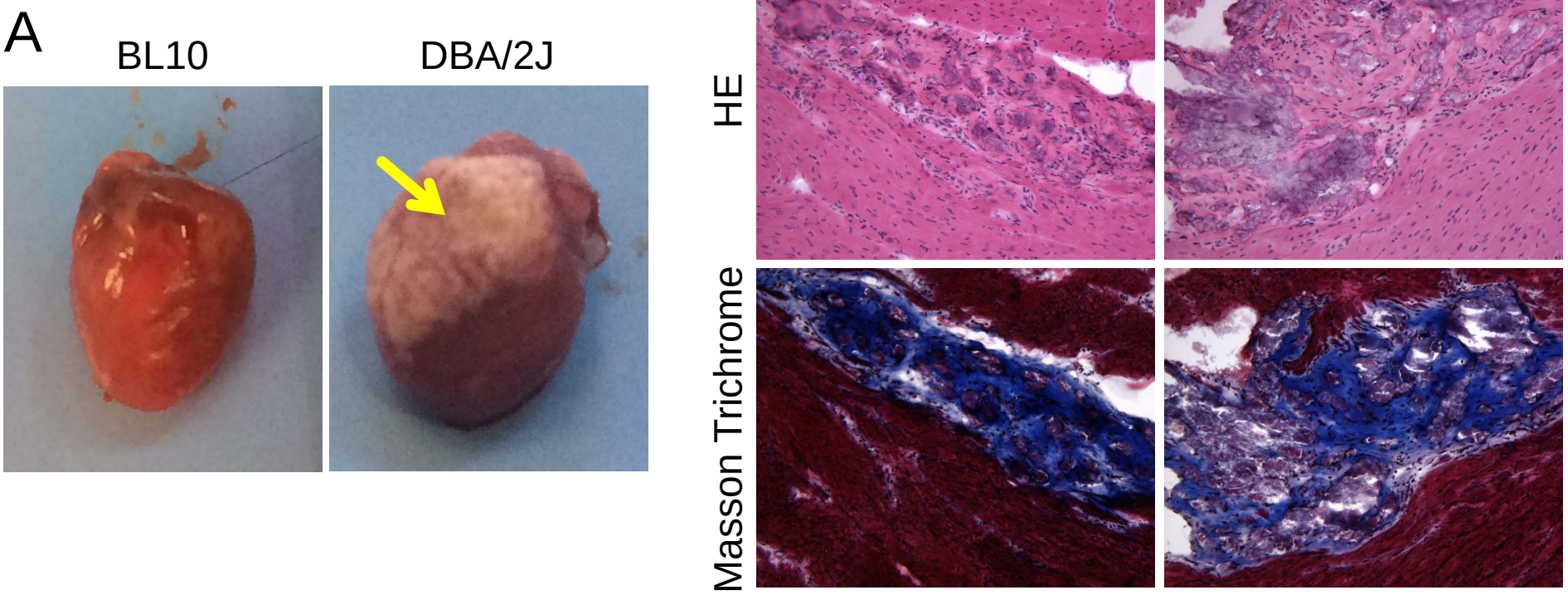

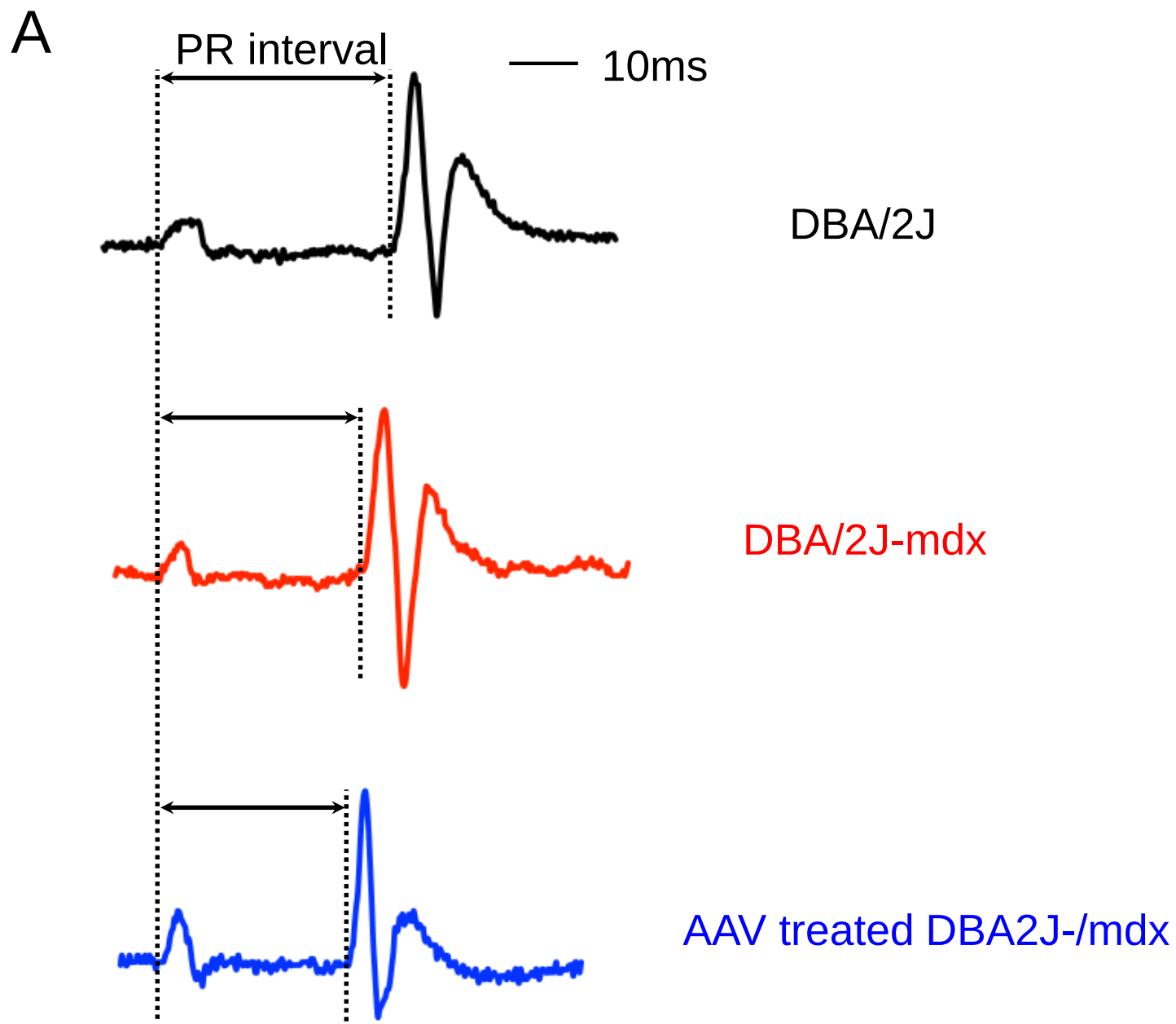
A
PR interval
10ms
DBA/2J
DBA/2J-mdx
AAV treated DBA2J-/mdx

Hakim et al. 2017 Figure S6B

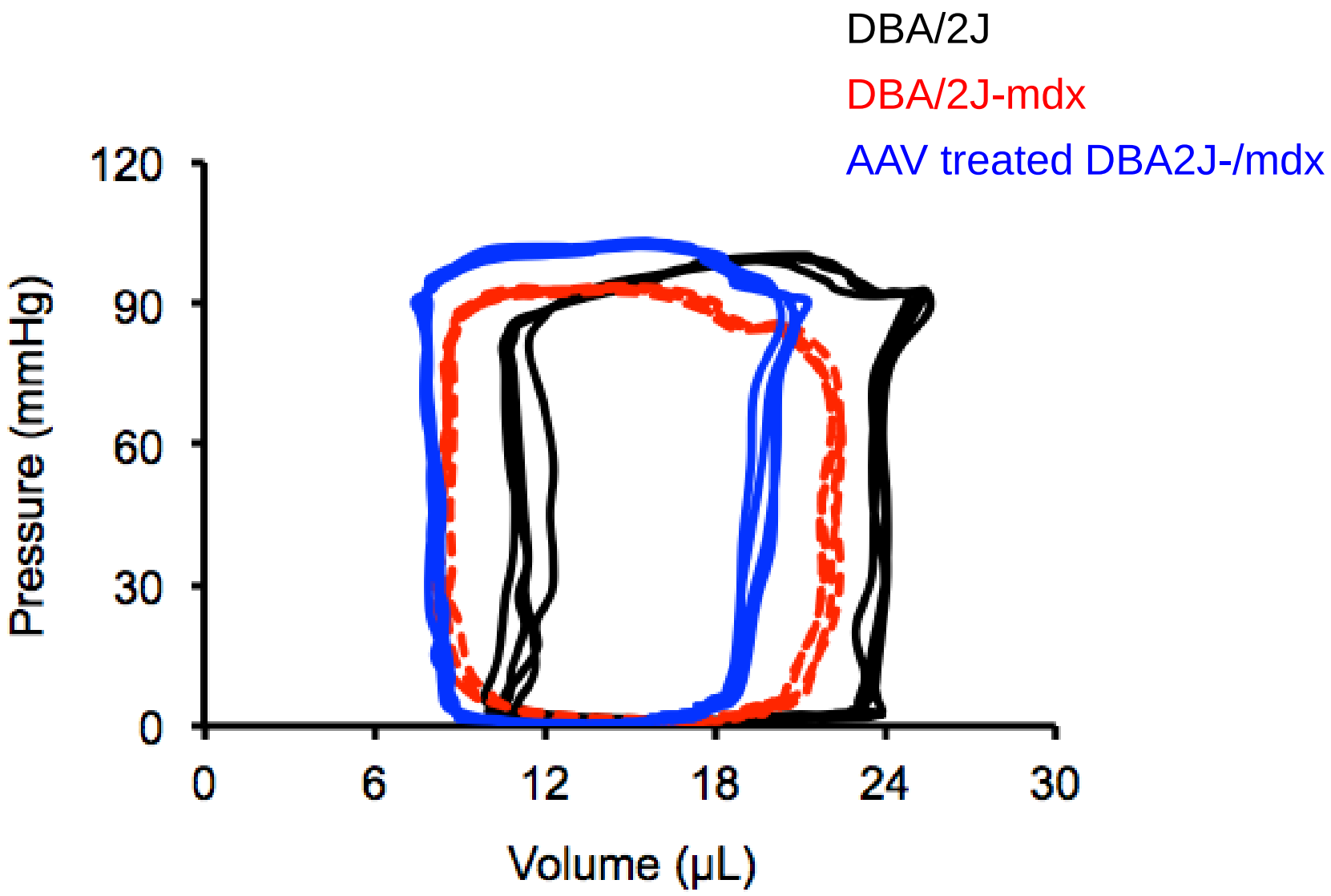

Supplemental Figure Legends

Figure S1. Widespread micro-dystrophin expression in skeletal muscle and the heart of AAV-9 treated DBA/2J-mdx mice. A, Representative photomicrographs of dystrophin immunostaining of the tibialis anterior muscle (TA), quadriceps and diaphragm from five AAV injected mice and an untreated DBA/2J-mdx mouse. **B,** Representative photomicrographs of dystrophin immunostaining of the heart (Top panel, full-view images; Bottom panel, high-power images) from five AAV injected mice and an untreated DBA/2J-mdx mouse. **C,** Quantitative evaluation of AAV genome distribution in muscle and internal organs using in AAV microgene injected male DBA/2J-mdx mice (N=5). TaqMan quantitative PCR detects the junction of R1-R16. Dia, diaphragm; Gas, gastrocnemius; Quad, quadriceps; TA, tibialis anterior.

Figure S2. Micro-dystrophin expression reduces skeletal muscle disease in DBA/2J-mdx mice. A, Representative full-view photomicrographs of the HE stained quadriceps, tibialis anterior muscle (TA) and diaphragm from untreated and AAV injected DBA/2J-mdx mice. Scale bar, 500 μm. **B,** Representative high-magnification photomicrographs of the HE stained quadriceps, TA and diaphragm from untreated and AAV injected DBA/2J-mdx mice.

Figure S3. Intravenous AAV-9 delivery results in saturated micro-dystrophin expression in the extensor digitorum longus muscle in DBA/2J-mdx mice. Representative full-view photomicrographs of dystrophin immunostaining from DBA/2J. DBA/2J-mdx and treated DBA/2J-mdx mice.

Figure S4. AAV micro-dystrophin therapy improves absolute muscle force of DBA/2J-mdx mice. A, Quantitative evaluation of the absolute twitch force and absolute maximal tetanic force in the extensor digitorum longus muscle (EDL). **B,** Quantitative evaluation of the absolute twitch force and absolute maximal tetanic force in the tibialis anterior (TA) muscle. Asterisk, untreated DBA/2J-mdx mice is significant different from that of DBA/2J and AAV treated DBA/2J-mdx mice. Cross, DBA/2J is significant different from that of AAV treated DBA/2J-mdx mice.

Figure S5. DBA/2J mice show spontaneous muscle pathology. A, Representative photomicrographs of freshly dissected BL10 and DBA/2J mouse hearts. Arrow indicates epicardial calcification and/or fibrosis on the surface of the right ventricle in the DBA/2J mouse. **B,** Representative high-magnification photomicrographs of HE and Masson trichrome-stained heart sections from DBA/2J and DBA/2J-mdx mice.

Figure S6. Representative ECG and the pressure-volume loop tracing from experimental mice. A, ECG reveals the shortened PR interval in a DBA/2J-mdx mouse. Micro-dystrophin therapy did not increase the PR interval. **B,** The pressure-volume loop shows a similar hemodynamic profile in DBA/2J and DBA/2J-mdx mice.